JOURNAL OF PETROLOGY | VOLUME 47 | NUMBER 3 | PAGES 567–593 | 2006 | doi:10.1093/petrology/egi086

Fluid Transfer in High-grade Metamorphic Terrains Intruded by Anorogenic Granites: The Thor Range, Antarctica

KURT BUCHER[1]* AND B. RONALD FROST[2]

[1]INSTITUTE OF MINERALOGY AND GEOCHEMISTRY, UNIVERSITY OF FREIBURG, ALBERTSTR. 23B, D-79104 FREIBURG, GERMANY

[2]UNIVERSITY OF WYOMING, DEPARTMENT OF GEOLOGY AND GEOPHYSICS, PO BOX 3006, LARAMIE, WY 82071-3006, USA

RECEIVED FEBRUARY 7, 2003; ACCEPTED OCTOBER 21, 2005
ADVANCE ACCESS PUBLICATION DECEMBER 7, 2005

A composite intrusive igneous complex in the central mountain range of Queen Maud Land (Thor Range), Antarctica, displays characteristic features of anorogenic granites. A suite of massive intrusives and various sets of dykes and satellite intrusions are ferroan, alkalic to alkali–calcic, and weakly peraluminous. An early set of plutons consists of charnockitic alkali-granites; a later group of plutons comprises fayalite Qtz-syenites. Coarse mesoperthite is the dominant mineral in all rocks, quartz is abundant and plagioclase is a minor mineral. Olivine (fayalite) is the characteristic mafic mineral, but subcalcic augite and occasionally pigeonite or orthopyroxene are present. In most samples, amphibole is the dominant mafic mineral and its composition is close to end-member hastingsite. It contains high concentrations of F and Cl. Some samples contain igneous fluorite. Thermobarometry suggests a temperature of 900 ± 25°C and a pressure of 0·4 ± 0·1 GPa for the crystallization conditions of the pyroxene–olivine assemblages. The solidus temperature of 800–850°C for both suites of plutonic rocks is typical of water-deficient granitic melts. The estimated low water activity of 0·3–0·5 at solidus conditions is consistent with the high halogen content of the bulk-rocks and their constituent minerals. In the absence of an aqueous fluid, the halogens remained in the minerals at the solidus. Oxygen fugacity stayed below QFM in all igneous rocks above solidus. This is typical of melts derived from partial melting of mafic source rocks. The igneous rocks were locally affected by at least three distinct episodes of hydration. As the melt approached solidus conditions, fayalite and pyroxene were locally transformed into hastingsite as a result of increasing fugacity of volatile components. Fayalite-free and fayalite-bearing igneous rocks are arranged in banded structures. Subsolidus hydration locally modified the igneous rocks and transformed pyroxene- and fayalite-bearing granites into biotite-granites and hornblende-granites in which all evidence of former high-T history was erased. This local hydration of igneous rocks occurred in response to uptake of H_2O that had been given off by gneissic xenoliths as a result of progressing, continuous, dehydration reactions. The reactions in the gneiss xenoliths were driven by contact metamorphism. This exchange of H_2O between igneous and metamorphic rocks occurred in a fluid-absent regime at temperatures of about 750°C. Late reaction veins formed by hydraulic fracturing of the plutonic rocks and indicate the presence of a low-density fluid phase at amphibolite facies conditions.

KEY WORDS: *anorogenic granite; fayalite; hastingsite; fluid recycling; Antarctica*

INTRODUCTION

Anorogenic granites form extensive, complexly structured, composite plutons predominantly in Precambrian shields but also in Phanerozoic rift systems (Haapala & Rämö, 1999; Bonin, 2005; Wahlen, 2005). They are distinguished from other types of granites by high-K (high-Na), high-Si, high-X_{Fe}, REE and halogens. Because of the extremely high Fe/Mg ratio of such granites, fayalite, hedenbergite and hastingsite are common mafic minerals. The granites typically formed under conditions of low H_2O pressure and reducing conditions ($fO_2 <$ QFM). Consequently, solidus temperatures are high (800–900°C) and the granites contain high-*T* feldspars.

*Corresponding author. E-mail: bucher@uni-freiburg.de

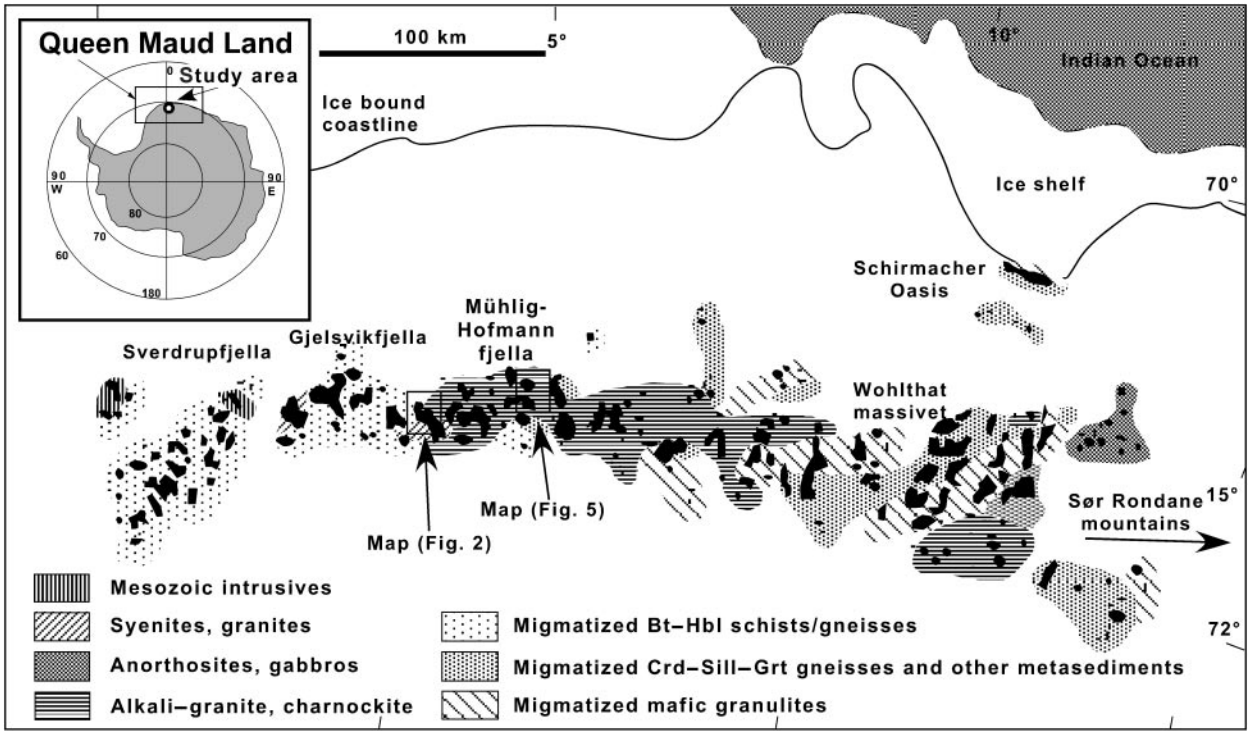

Fig. 1. Simplified geology of the Thor Range after Ravich & Solov'ev (1966). Outcrop area shown in black, glaciers and shelf ice in white; place names as used in the text; inset indicates location of Queen Maud Land; rectangles indicate the local geological maps in Figs 2 and 3.

These common elements of anorogenic granites suggest a similar petrogenesis. Anorogenic granites are typical of geodynamic settings in which lithospheric extension plays an important role (e.g. Haapala & Rämö, 1992); however, other settings seem possible as well (Bonin, 2005; Wahlen, 2005). The hot and water-poor granitic melts that formed the plutons suggests a mechanism of formation in which a primary basaltic heat source triggers anatexis of lower crustal source material (Frost & Frost, 1997; Frost *et al.*, 1999).

A large igneous province on the East Antarctic shield is composed of granite plutons showing characteristic chemical and mineralogical features of anorogenic granites (Fig. 1). The complex composite plutons underlie extensive outcrop areas of the mountain range of central Queen Maud Land (Ravich & Solov'ev, 1966; Ohta *et al.*, 1990; Ohta, 1993; Ravindra & Pandit, 2000). The plutons are generally composed of granites and Qtz-syenites and contain augite, hastingsite and fayalite as primary mafic minerals. The massive to weakly foliated Qtz-syenites and granites locally contain orthopyroxene and consequently may also be termed charnockites (Ohta *et al.*, 1990; Frost & Bucher, 1993). Several generations of granitoid rocks can be distinguished on the basis of textures and cross-cutting relationships.

The magmas intruded Precambrian continental crust composed of migmatitic gneisses and various metasedimentary rocks, including metapelites and marbles (Grantham *et al.*, 1991; Groenewald & Hunter, 1991; Tingey, 1991; Bucher-Nurminen & Ohta, 1993; Markl & Piazolo, 1998; Piazolo & Markl, 1999), at depths of about 10–15 km (Bucher-Nurminen & Ohta, 1993). The resulting high-temperature contact metamorphism is locally preserved and fluids released by the metamorphic reactions interacted with both the magmas and with the igneous rocks at subsolidus conditions. The complex effects ensuing from fluid release, fluid transfer and fluid consumption on both the crystallizing igneous rocks and the contact metamorphic country rocks is the main subject of this communication.

High-temperature assemblages of igneous and metamorphic rocks tend to be vulnerable to retrogression by nomadic fluids. They may be fully replaced by assemblages at lower temperature leaving no trace of the high-grade past of the rocks. The effect of resetting the high-grade assemblages on thermobarometry is known as the granulite uncertainty principle (Frost & Chacko, 1989; Bucher & Frost, 1993). Fluid–rock interaction partially erased high-grade assemblages in igneous and metamorphic rocks of the Thor Range in complex structural patterns that allow for a better understanding of fluids in high-grade processes (Dallmann *et al.*, 1990; Frost & Bucher, 1993; Bucher & Frost, 1995).

REGIONAL GEOLOGY

The Thor Range of Antarctica extends about 600 km from west to east, parallel to the coast of the Weddell Sea (Fig. 1). It comprises a Mid- to Late-Proterozoic basement that was overprinted by an orogenic event in the early Palaeozoic (Roots, 1969; Allen, 1991; Tingey, 1991). The basement consists of quartzo-feldspathic gneisses, tonalitic to granitic gneisses, migmatites and high-grade metasediments, including metapelites and widespread marbles and calc-silicate rocks (Groenewald & Hunter, 1991; Moyes *et al.*, 1993). The entire sequence of rocks was complexly folded and deformed during an orogenic phase at 1·0–1·2 Ga (Paulsson & Austrheim, 2003).

Moyes & Groenewald (1996) reported early Palaeozoic garnet Sm–Nd ages for Precambrian gneisses in western Queen Maud Land, which suggest amphibolite to granulite facies conditions during an early Palaeozoic thermal phase (Pan-African). The early Palaeozoic East Antarctic orogen may represent the southern continuation of the East African Mozambique belt (Jacobs *et al.*, 1998; Piazolo & Markl, 1999) formed by collision of East and West Gondwana in Neoproterozoic to early Palaeozoic times (580–515 Ma). It also was suggested that the western front of this orogen could be delineated at Heimefrontfjella to the west of our working area on the basis of distinct magnetic structures in the crust (Golynsky & Jacobs, 2001).

The central portion of Thor Range was intruded by large plutons of Qtz-syenite, alkali-granite and granite during the early Paleozoic. Intrusion ages of 500 Ma for the plutonic rocks are well documented (Ohta *et al.*, 1990; Henjes-Kunst & Markl, 1998; Jacobs *et al.*, 1998; Paulsson & Austrheim, 2003). The igneous province extends to eastern Mühlig-Hofmannfjella and further eastwards with apparently similar overall chemical characteristics. Henjes-Kunst & Markl (1998) and Markl & Piazolo (1998) presented data from the Wohlthat mountains where granites were emplaced at $P = 500$ MPa and $T = 900$°C and contain F- and Cl-rich late amphibole and biotite. The authors reported evolution from water-deficient granitic melts to water-saturation at 800°C. Their age data suggest a period of igneous activity of 100 Ma duration (from 610 to 500 Ma). Ravindra & Pandit (2000) reported anorogenic granites from the Northern Humboldt Mountains in the Wohlthat Group (Fig. 1). An Rb–Sr whole-rock isochron gave 514 ± 59 Ma. Biotite and hornblende are the predominant mafic minerals but some samples contain Cpx and Opx. The suite of plutonic rocks belongs to the syenogranite and monzogranite family. Also typical is high X_{Fe}, A/CNK varies between 0·86 and 0·99; this metaluminous bulk-rock composition is associated with high K/Na and enrichment in REE.

At the western edge of the igneous province, Paulsson *et al.* (1999) reported U–Pb zircon ages of about 500 Ma (495, 501) from the LREE-enriched small Stabben syenite plug in Gjelsvikfjella (Fig. 1). The Stabben syenite has an anorogenic geochemical signature and intrudes a thick crust of gneissic basement of mid-Proterozoic age (Jacobs *et al.*, 1998; Paulsson & Austrheim, 2003).

The Thor Range igneous province also comprises smaller gabbro and anorthosite plutons (Fig. 1). The characteristic association of gabbro, anorthosite, syenite and granite and the compositional and mineralogical features of the plutonic rocks are typical of an anorogenic bimodal igneous suite (Rämö & Haapala, 1995). The plutons were emplaced after the early Palaeozoic orogenic event (Pan-African) in an anorogenic within-plate setting.

LOCAL GEOLOGY AND FIELD DATA

The plutonic complex of the central Thor Range is well exposed in Mühlig-Hofmannfjella (Fig. 1) and it has its western termination at 4°E (72°S) around Hoggestabben and Hochlinfjellet (Fig. 2). The studied localities are around Hochlinfjellet in the west (Fig. 2) and Svarthamaren in the east (Fig. 3). An extensive group of outcrops of plutonic rocks is also found in the area of Skigardene between Hochlinfjellet and Svarthamaren. The outcrops are typically steep alpine-type cliffs and walls rising several hundred meters above the surrounding ice (Figs 4 and 5). The elevation of the ice north of the mountain range is about 1700 m and the highest peaks are 2700 m; the ice sheet south of the mountain range reaches about 3000 m above sea level. The outcrops consist predominantly of Palaeozoic intrusives including granite, gabbro and syenite that intrude Proterozoic basement gneisses and metasedimentary rocks (Dallmann *et al.*, 1990; Ohta *et al.*, 1990; Bucher-Nurminen *et al.*, 1990; Ohta, 1993).

In the Hochlinfjellet area (Fig. 2), at least two major plutons are present. An early generation of intrusives consists of grey alkali-granite and charnockite. It locally contains numerous mafic inclusions of syenodiorite which form swarms of rounded or flattened xenoliths. The early alkali-granite suite was later intruded by fayalite-bearing Qtz-syenite to granite. The fayalite-granitoids form massive coarse-grained igneous rocks and fragmented the earlier plutons along the margins and formed megabreccias. The plutonic rocks locally also contain many inclusions of gneissic xenoliths. The angular blocks of gneiss, ranging from a few centimetres to tens of metres in size, show sharp contacts to the igneous rocks.

In the Svarthamaren area (Fig. 3), the intrusive relationships show that a late brown Fa-syenite intrudes earlier light-brown granite containing relics of

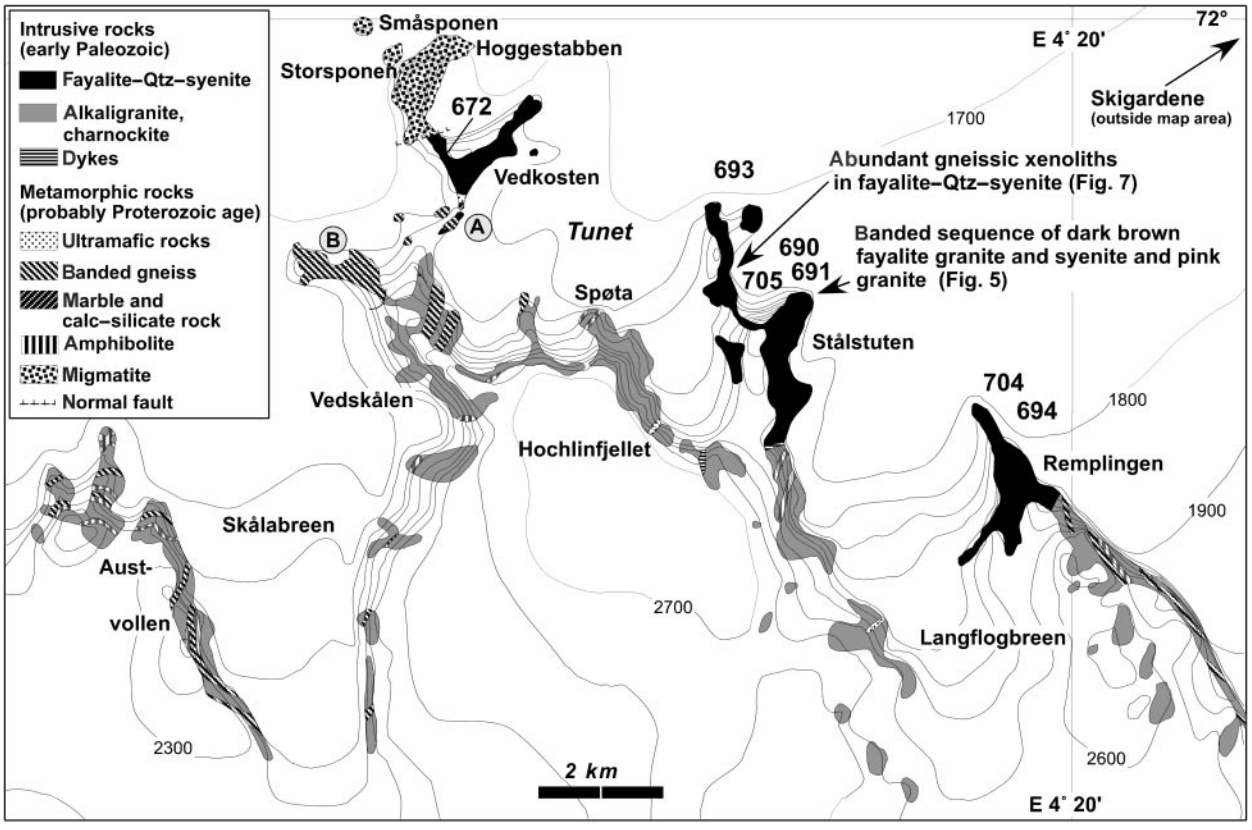

Fig. 2. Detailed geological map of the Tunet–Stålstuten–Remplingen fayalite–Qtz-syenite and alkali-granite complex [modified from Ohta (1993)]. Elevation contours in metres above sea level, place names and sample locations, with sample numbers as used in the text. Contact metamorphic metapelites at localities A and B described by Bucher-Nurminen & Ohta (1993).

orthopyroxene. A well exposed dyke system cuts across massive charnockite in the NE wall of Svarthamaren (Fig. 4). The dyke rocks show a wide variation as regards colour, grain size, texture, composition and mineralogy. The clear low angle normal faults exposed in the wall indicate syn-magmatic extensional tectonics. The outcrop also shows that the intrusion of the dykes occurred concurrently with brittle deformation (faulting) of the massive granite.

The cross-cutting relationships of intrusions and dyke systems show that an early generation of Fa–Opx-granite (charnockite) intrusions is followed by a later suite of fayalite-bearing Qtz-syenites (Dallmann *et al.*, 1990). The dyke system (Fig. 4) shows a consistent age hierarchy: the oldest generation of thick black mafic dykes consists of Opx-bearing syenodiorite (e.g. sample KB601). A younger system of thin dykes (e.g. KB636) consists of porphyric Opx-bearing granite. These early dykes are cross-cut by massive, up to 30 m thick dykes of granite (KB638) followed finally by a late thin (2 m) dyke generation that consists of fayalite- and fluorite-bearing alkali-granite (e.g. KB648 and KB649). The age relationships of the dykes (Fig. 4) suggest that the magma evolved from early syenodiorite to late alkali-granite. The dyke system is not restricted to the Svarthamaren area but has been observed at other localities with consistent age relationships. The youngest Qtz-syenite plutons do not contain a dyke system.

A striking field feature of the plutonic complex is the presence of igneous rocks of strongly contrasting colour, weathering and morphology. A brown, dark-coloured group of rocks forms pinnacles, needles and towers. It consists mainly of fayalite-bearing alkali-granites and Qtz-syenites. Another group of rocks forms dome-shaped peaks and consists of grey and pink granites. In some places, the two types of rocks are intimately associated and form irregularly banded mountains (Figs 5 and 6). Some of the contrasting bands in the Stålstuten N-face (Fig. 5) represent a sequence of intrusive Fa-syenite sheets in earlier alkali-granite. However, other portions of the dark-light banding are caused by different mineral assemblages present in rocks of similar bulk composition. Specifically, all dark-coloured igneous rocks contain fayalite. Weathering of the Fe-olivine produces iddingsite—a mixture of ferric hydroxides and hydrous silicates—that stains the rocks brown to dark-brown. The field relations

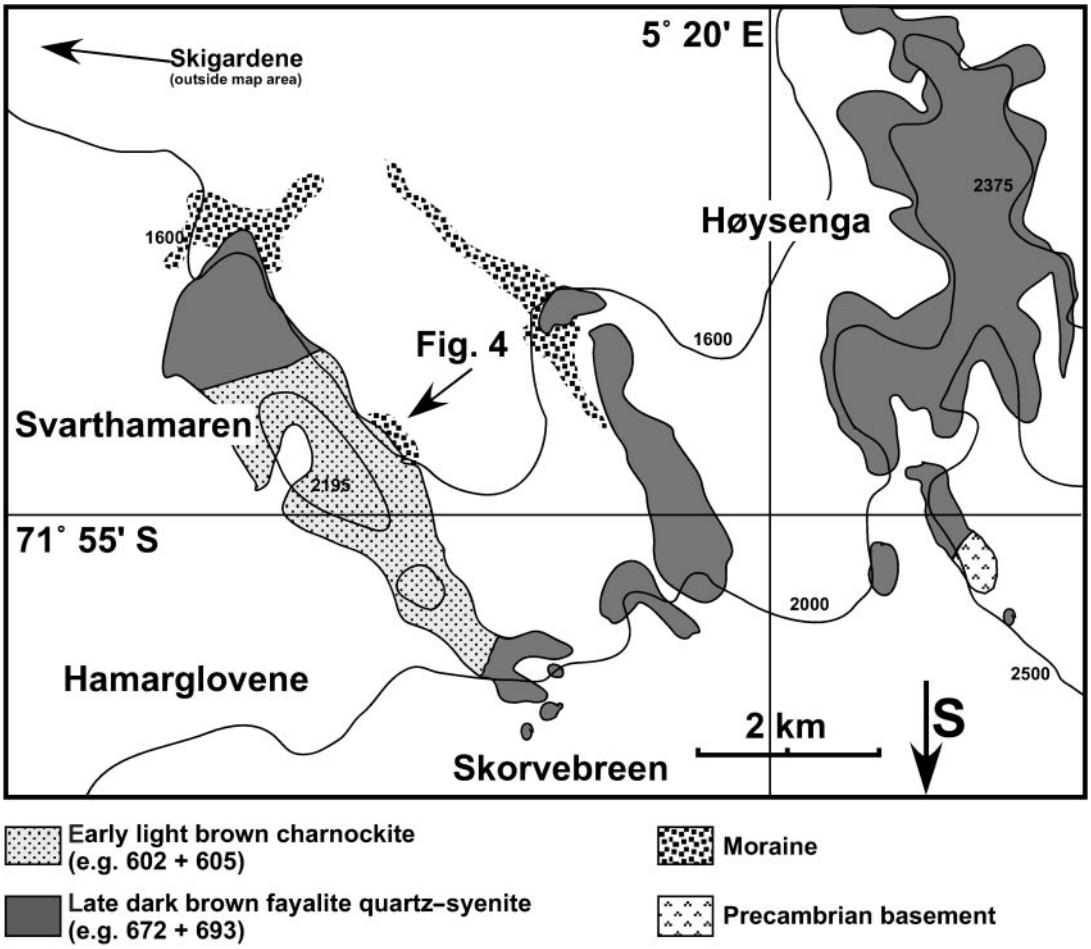

Fig. 3. Simplified geological map of the Svarthamaren granite (charnockite) complex [modified from Ohta (1993)]. Elevation contours in metres above sea level, place names as used in the text. Sample numbers of representative samples given in parentheses in key.

show (Fig. 6) that fayalite has been removed from the rocks during two different episodes. The first fayalite-consuming reactions produced pink Hbl–Bt granite in structures that are steeply dipping, irregular and patchy bands in dark fayalite granite (Fig. 6). A second outbreak of reaction discoloured brown fayalite-bearing granite and syenite along zones with abundant inclusions of country rock gneiss and other xenolith material and along vein-like structures originating at gneiss xenoliths (Figs 6 and 7). At some localities, the gneissic xenoliths in the dark-brown charnockite are surrounded by pink halos (Fig. 7). Pink fayalite-free granite surrounds the gneiss inclusions but also extend into veins and other, probably fracture-related structures. Brown fayalite-granite is locally in direct contact with gneiss and may have originally enclosed all gneiss xenoliths as primary igneous rock. The field relationships suggest that pink biotite-granite halos formed around the gneiss xenoliths and along a fracture network after the entrapment of the gneiss fragments in the primary magma. This, in turn, consequently implies that the late pink–grey biotite–orthoclase–Qtz rock formed from the dark fayalite-bearing granite. The field observations (Fig. 7) indicate that removal of fayalite from the igneous fayalite-granite occurred in response to a reactive component provided by the gneiss inclusions in the igneous rocks. Fayalite loss in the granite directly surrounding the gneiss xenoliths makes this granite unable to later develop iddingsite, the brown stain of Fa-granite. As a consequence, its light pink weathering colour contrasts with the dark-brown colour of Fa-granite. The irregular patchy boundary between fayalite-granite and hornblende-biotite granite thus represents the front of a fayalite-consuming reaction driven by a component given off by the gneiss xenoliths.

Some gneiss inclusions in fayalite-granite do not display a discoloration halo around them (Fig. 8). The gneiss fragments show sharp angular outlines and sharp boundaries to the enclosing fayalite-granite without visible evidence of interaction between the two types of rock.

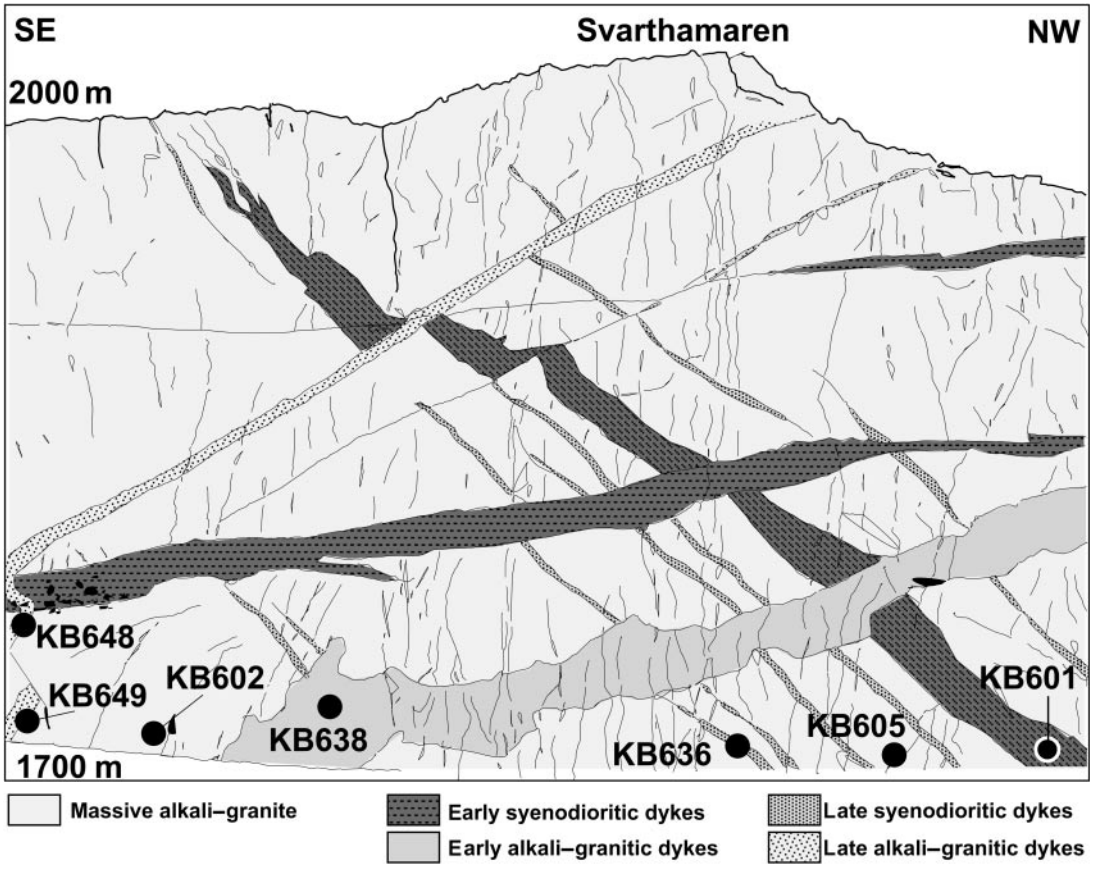

Fig. 4. Sketch of the NE face of Svarthamaren. The massive wall consists of homogeneous alkali-granite with relics of Opx. A large number of different types of dyke rocks cut across the wall; the cross-cutting relationships show that an early set of dark syenodioritic dykes (KB601) is followed by brown syenodiorites (KB636), early grey alkali-granite dykes (KB638) and finally by the latest alkali-granite dykes (KB648, KB649). The vertical face of the cliff is 300 m high. Samples were collected at the foot of the wall at the numbered localities.

No migmatite structures related to partial melting during contact metamorphism have been observed in the gneiss xenoliths. Note that some gneisses are Proterozoic migmatites (Fig. 8), the migmatite structures are geometrically unrelated to the shape of the xenoliths and leucosomes (partial melts) never cross the xenolith's boundary. The observations indicate that some country rock fragments were capable of releasing a reactive component, whereas others were not. The xenoliths show no evidence of *in situ* partial melting and migmatitic structures are inherited from their Proterozoic past.

PETROGRAPHY

Igneous rocks

Mineral assemblages in the granitoid plutonic rocks (Table 1) from localities between Stålstuten in the west (Fig. 2) and Svarthamaren in the east (Fig. 3) are modally dominated by euhedral, transparent, dark honey-coloured, mesoperthitic alkali feldspar, ranging in size from a few millimetres to several centimetres. Coarse exsolution textures are widespread. Mesoperthite and coarse anhedral quartz form about 80 vol. % of many of the rocks (Fig. 9a). If present, plagioclase in the same rock has much smaller grain size and forms discrete grains in the matrix (Fig. 9a).

Olivine, subcalcic augite, pigeonite and orthopyroxene occur in different associations. Olivine is the most abundant Fe–Mg silicate in some rocks and may exceed 10 vol. % in some samples. The rocks can, therefore, be classified as fayalite-granites; however, the term 'charnockite' is also correct because the diagnostic association orthopyroxene + Qtz occurs in the fayalite-granite. Olivine is always slightly altered and alteration products include serpentine and Fe-hydroxides, -oxides and -carbonates (iddingsite). Brown-coloured Fa-syenite has its colour from some degree of iddingsitization and the Fe-hydroxides stain the rocks brown at the outcrops. In many samples, the degree of alteration is low and olivine is well preserved (Fig. 9b). In other samples, olivine may be severely corroded and altered to brown iddingsite (Fig. 9c). Olivine is absent in the grey–pink

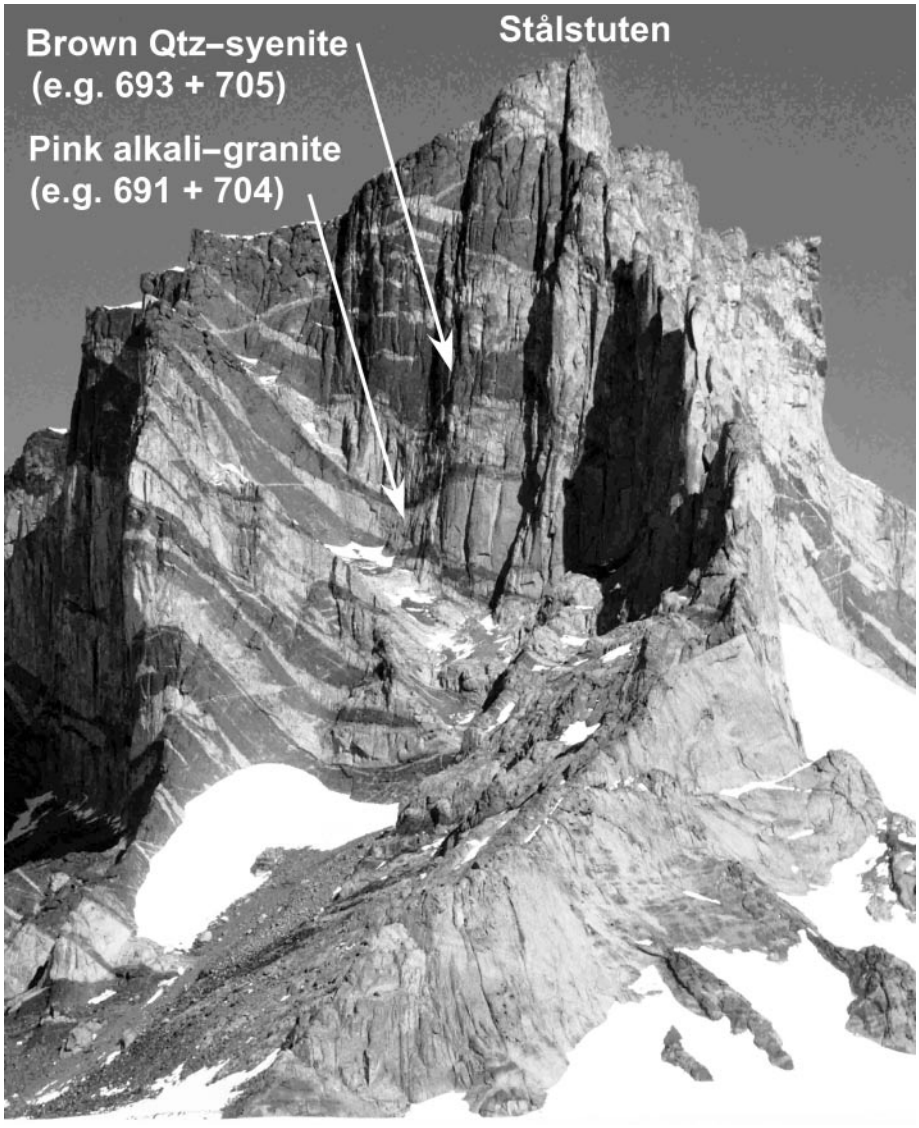

Fig. 5. Stålstuten (2608 m) seen from NE (location Fig. 2). Dark bands, brown Fa–Qtz-syenite with mesoperthite–Qtz-plagioclase–olivine ± pyroxene; light bands, pink alkali-granite with K-feldspar–Qtz–plagioclase–hornblende–biotite and opx relics. Height of the outcrop: 900 m. Sample numbers of representative samples given in parentheses.

Bt–Hbl-granites. Pyroxene is less abundant than olivine. Three varieties of pyroxene were found: orthopyroxene, augite and, in two samples, inverted pigeonite (Table 1). Subcalcic augite is the typical clinopyroxene of the rocks (Fig. 9d). Inverted pigeonite shows typical coarse exsolution lamellae of subcalcic augite in an orthopyroxene matrix (Fig. 9e). The absence of reaction textures between olivine and pyroxene may suggest that they represent coexisting magmatic phases. The mafic minerals are texturally later than the dominant euhedral large mesoperthite. Orthopyroxene occurs in fayalite-free rocks and it is commonly partially resorbed and overgrown by later biotite.

In addition to the anhydrous minerals, most samples contain amphibole and (or) biotite (Table 1). None of the fayalite-bearing granitoids contains biotite, however (except for two alkali-granite dykes). The coarse anhedral interstitial amphibole is a hastingsite (see mineral chemistry). In some samples, hastingsite coexists with the anhydrous phases in equilibrium textures; in others, clear reaction textures suggests that hastingsite forms from anhydrous Fe–Mg minerals (Fig. 9f and g). The pink granite contains biotite and amphibole but no anhydrous Fe–Mg silicates. Myrmekite textures and fine Bt + Qtz intergrowth textures are common in most samples. In most samples, REE-rich allanite is an

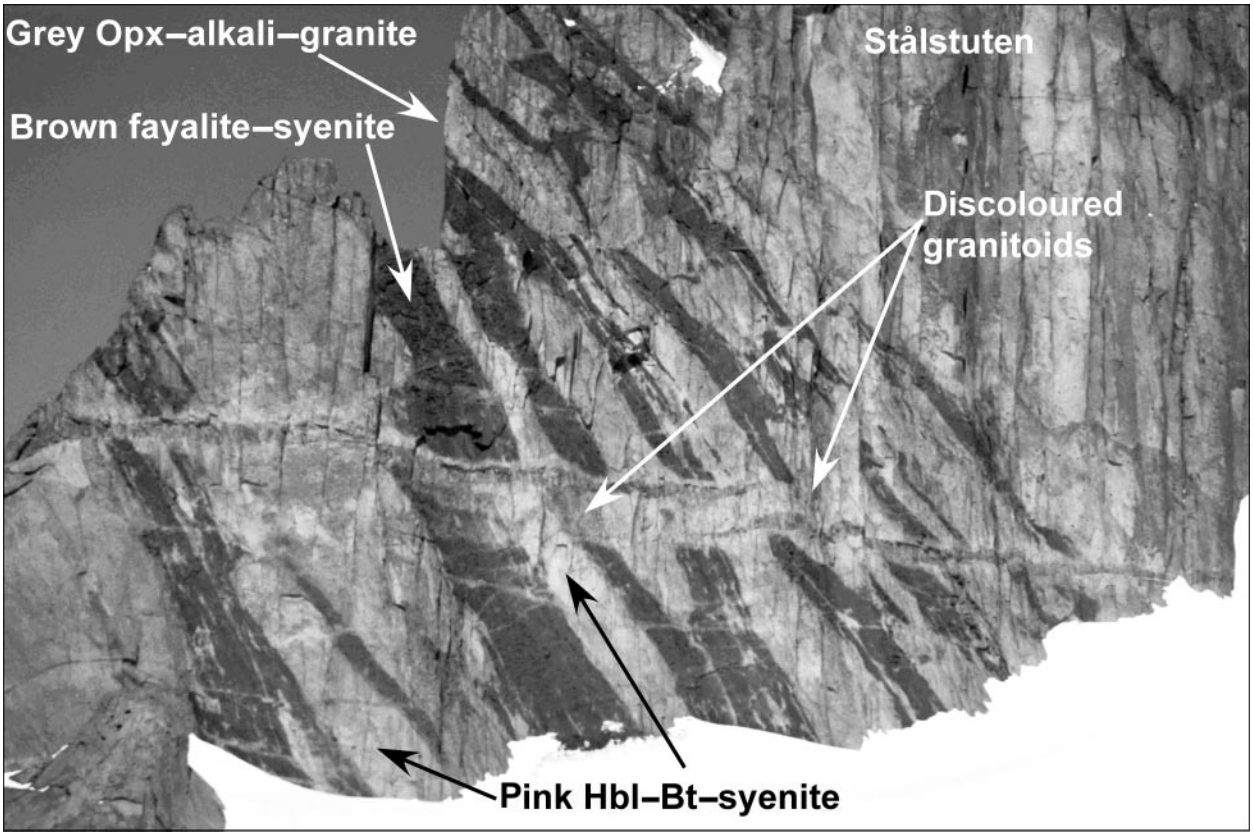

Fig. 6. Banded outcrop at Stålstuten (location Fig. 2) with brown fayalite–Qtz-syenite and pink Hbl Bt-granite, local occurrence of grey alkali-granite (charnockite). Late, fluid-induced discoloration of all lithologies along horizontal structures.

abundant minor phase. Ilmenite is the common primary opaque phase. Abundant magnetite typically forms irregular masses and rinds overgrowing olivine. The textures indicate that magnetite may not be a phase of the solidus assemblage but rather formed later by subsolidus processes. Apatite and zircon are common accessory minerals. Interstitial fluorite is present in two fayalite-bearing alkali-granite dykes (KB648, KB649). It coexists with hastingsite and biotite in apparent equilibrium textures (Fig. 9h), suggesting that fluorite is a member of the solidus assemblage in these rocks.

The modal composition of the plutonic rocks falls into three distinct groups: (1) a large group are typical alkali-granites; (2) a second group contains very little quartz and consequently belongs to the syenite family of rocks (syenogranites, syenites and Qtz-syenites); and, finally, (3) a third group of rocks with intermediate modal composition on a QAP diagram (Fig. 10). The modal QAP variation is not continuous and there are three distinct groups. The alkali-feldspar to plagioclase ratio does not change much in the intrusives. The modal composition of some of the dyke rocks is quite different from the plutonic rocks. The earliest generation of dykes is Qtz-monzonite; the intermediate dyke generation is similar to the intermediate plutonic rocks, whereas the latest dykes contain very little plagioclase.

Xenoliths and country rocks

The intruded basement and its disrupted fragments enclosed in the plutonic rocks consist of felsic and mafic gneisses, quartzite, calc-silicate rocks and marbles. The banded gneissic rocks contain layers of metapelite made of the minerals garnet, K-feldspar, plagioclase, cordierite, biotite, sillimanite and, locally, orthopyroxene (not together with sillimanite) in a variety of assemblages (Bucher-Nurminen & Ohta, 1993). Hercynite is present in some samples, but exclusively as inclusions in cordierite, sillimanite and plagioclase. Microstructures suggest that the oldest assemblage with garnet + K-feldspar was later replaced by assemblages including orthopyroxene and cordierite, and, at an even later stage, with biotite + sillimanite (Bucher-Nurminen & Ohta, 1993). Felsic gneisses typically contain the assemblage garnet + biotite + sillimanite + Qtz + plagioclase + K-feldspar. However, sillimanite is lacking in the most common and widespread rusty garnet–biotite gneisses.

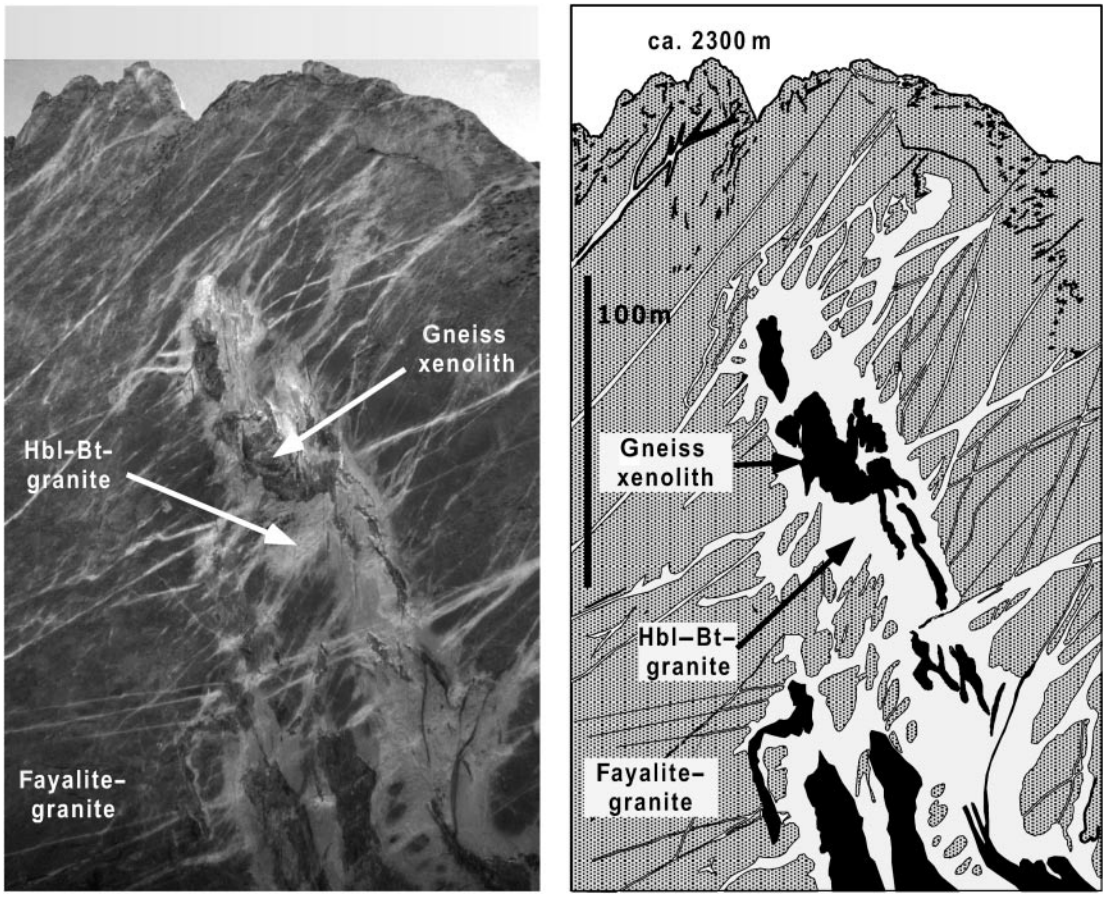

Fig. 7. Photograph and schematic drawing of the east face of the northern extension of Stålstuten (location Fig. 2) showing discoloration halos around gneiss xenoliths in Fa-granite. Dark shades represent dark brown Fa-granite with mesoperthite–Qtz–plagioclase–olivine ± pyroxene; light shading represents pink granite with K-feldspar–Qtz–plagioclase–biotite ± hornblende. The light veins (granites) represent former Fa-granite that has been hydrated by late hydrous fluids. Gneissic xenoliths contain plagioclase–hornblende–clinopyroxene–orthopyroxene–biotite ± Qtz.

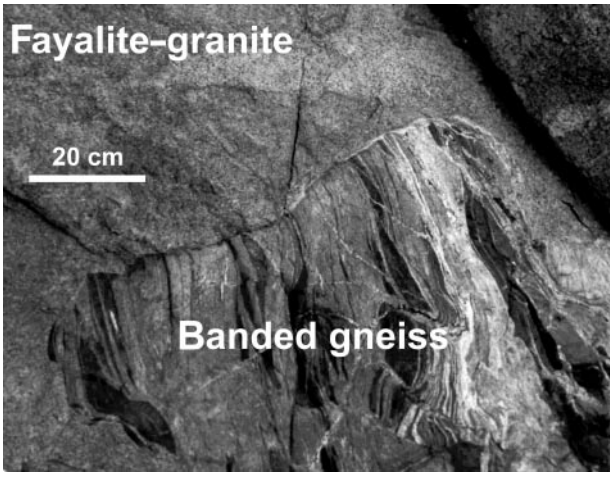

Fig. 8. Gneiss inclusions in fayalite-granite at Stålstuten. Discoloration halos are absent; partial melting structures related to contact metamorphism by the fayalite-granite are not present.

Contact metamorphic mafic gneisses contain assemblages involving plagioclase, quartz, biotite, amphibole, garnet, orthopyroxene and clinopyroxene (Table 2). The two-pyroxene assemblage of the mafic gneisses corresponds to the orthopyroxene–garnet–cordierite assemblage in the felsic gneisses. Xenoliths of mafic gneiss in the plutonic rocks show clear textural evidence of prograde hornblende decomposition. Amphibole is replaced by two pyroxenes and plagioclase (Fig. 11a–c). The mafic granulites developed late biotite from orthopyroxene (Fig. 11d), analogous to the formation of biotite + sillimanite assemblages from garnet + cordierite in the felsic gneisses. Amphibole-overgrowths on pyroxene are rare.

Marbles and calc-silicate rocks are present as blocky fragments in plutonic rocks and in country rocks, in addition to the gneisses. The rocks contain calcite, plagioclase, scapolite, clinopyroxene, grossular, phlogopite and titanite in a number of different assemblages. Tremolite locally replaces Cpx (diopside) as a late phase. At

Table 1: Qtz-syenites, alkali-granites and dyke rocks: mineral assemblages, qualitative relative abundance and texture data

Rock	Sample	Locality	Msp	Pl	Qtz	Ol	Opx	Cpx	Hbl	Bt	Other	Colour
Alkali-granite	85BT104	HS	XX	x	X	x		x			Ilm, Idd	brn
	90YOA18	HS	XX	X	X		x	x			Pgt	l-brn
	KB614	SG	XX	x	X	X			x*		Idi, Mag, Ilm	brn
	KB602	SH	XX	(x)	X					x	Zrn, My, Mag, Ilm	l-brn
	KB605	SH	XX	(x)	X		x^r			x	Zrn, My, Mag, Ilm	l-brn
	85BT48	SH	XX	x	X		x	x		x	Ilm	l-brn
	85BT98	SH	XX	x	X		x	x	x		Pgt, Ilm	l-brn
	85BT115	SH	XX	x	X	x	x	x			Ilm, Idd	brn
	85BT144	SH	XX	x	X		x		x	x	Ilm	brn
	KB690	SS	XX	x	X				X	(x)	Aln	pink
	KB691	SS	XX	x	X				x	X	Aln	pink
	KB704	SS	XX	x	X		x^r		x	x	Aln	pink
Syenite	KB672	HO	XX	X	(x)	X		x	x		Idd, My, Mag, Ilm	brn
	KB693	SS	XX	x	(x)	X		X	x		Idd, My, Zrn, Ap, Ilm, Mag	brn
	KB694	SS	XX	x	X				X	x	Ilm, Mag, Zrn	pink
	KB705	SS	XX	x	X	x			x		Aln, Idd	brn
Dyke rock	KB601	SH	x	X	X	x	X		x	x	Idd	black
	KB636	SH	XX**	x	X		x^r		x	x	Aln, Mag, Ilm	brn
	KB638	SH	X	X	X				x	x	Aln, Ap, Ilm, Zrn	grey
	KB648	SH	XX	x	X	X			X*	x	Aln, Idd, Zrn, Ap, Ilm, Flt, Mag	brn
	KB649	SH	XX	x	X	x^r			X*	x*	Aln, Idd, Mag, Ilm, Ap, Flt	brn

XX, >50% mode; X, major phase; x, minor phase; (x), very small amount; ^{r}relic phase; *Cl-amphibole; **coarse porphyric orthoclase locally microperthite; samples KB704 and KB705 were donated by H. Austrheim; Msp, mesoperthite; Idd, iddingsite; My, myrmekite; other mineral names from Bucher & Frey (2002); SH, Svarthamaren; HS, Høgsenga; SS, Stålstuten; HO, Hoggestabben; SG, Skigardane; YO and BT samples from Ohta *et al*. (1990); brn, brown; l-brn, light-brown.

one locality, very coarse-grained wollastonite occurs as continuous layers between marble and quartz-bearing intrusive rocks and armours calcite from direct contact with quartz.

ANALYTICAL METHODS

The composition of 15 samples of igneous rocks was analysed by XRF (X-ray fluorescence) using a Philips 2404 spectrometer operating at 30 kV and 40 nA (Table 3). Fused beads were used for major elements, and powder pellets for trace elements. Loss on ignition (LOI) was determined to complete the XRF analyses. Total Fe is reported as Fe^{2+}.

Mineral compositions were determined by electron probe microanalysis (EPMA) using the JEOL 8600 Superprobe at the University of Basel, a CAMECA CAMEBAX instrument at the University of Wyoming and a CAMECA SX100 instrument at the University of Freiburg, respectively. All quantitative analyses were made using the wavelength dispersive spectrometers of the three instruments. The acceleration voltage was 15 kV, the beam-current was 10 nA and the counting times were 10 s. Analyses were made using a focused electron beam (spot size = 2 μm), except for Na and K measurements in mica and amphibole and for measuring alkali-feldspar with fine exsolution of Na-feldspar where a defocused beam has been used (~10 μm). The instruments were calibrated for each element analysed using well characterized natural materials as standards. Data reduction was performed by utilizing software provided by the manufacturers of the three instruments.

COMPOSITION OF THE IGNEOUS ROCKS

In the classification scheme of Frost *et al.* (2001), most samples are ferroan alkalic metaluminous granitoids; a few of the syenites and the most siliceous granites and some of the dykes are alkali calcic. The most siliceous granites are also very weakly peraluminous. The SiO_2 content of the plutonic rocks varies between 59 and 76 wt % (Table 3). On the $K_2O + Na_2O$ vs SiO_2 diagram

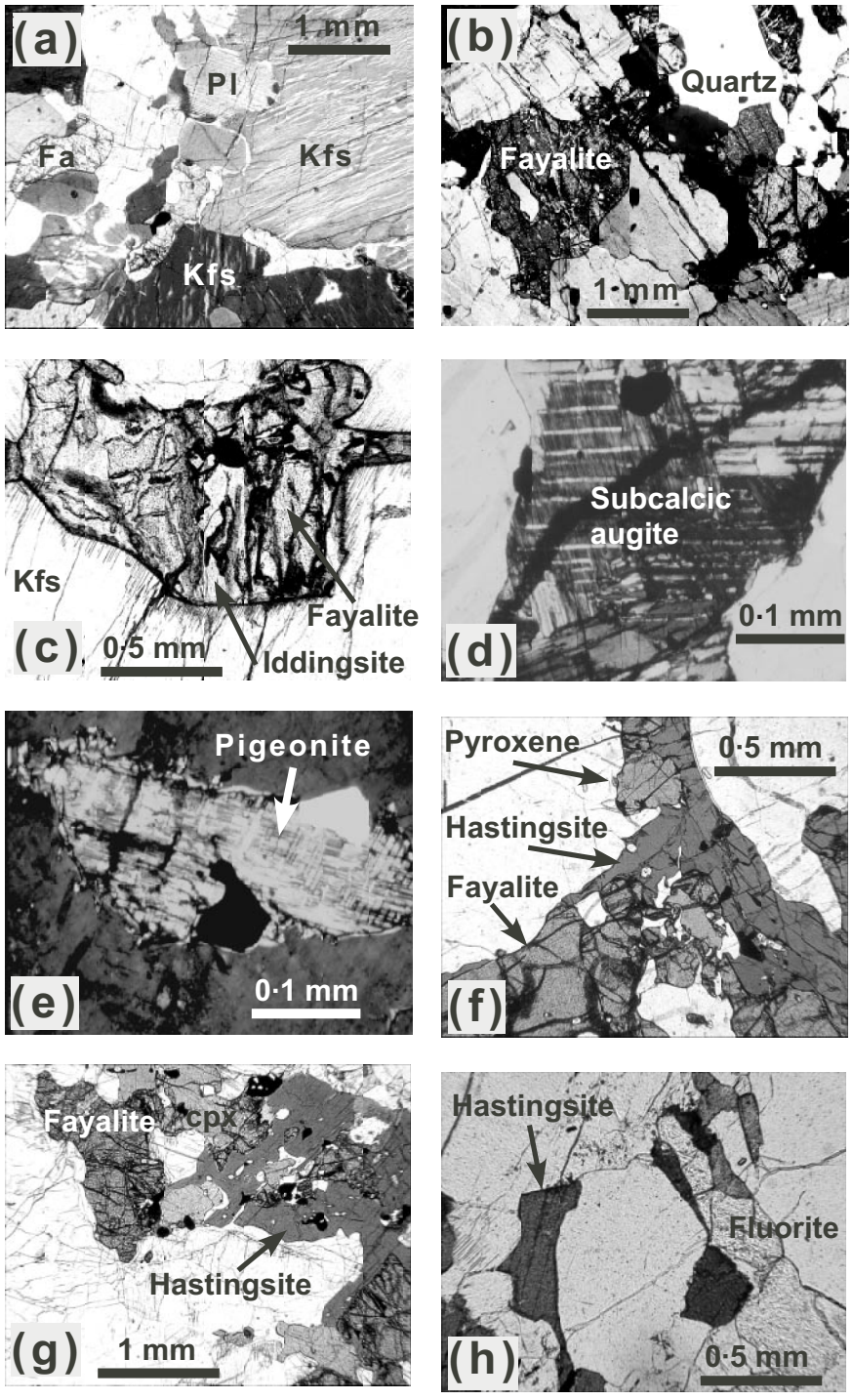

Fig. 9. Photomicrographs of igneous rocks: (a) KB705: olivine, coarse mesoperthite and smaller plagioclase; (b) KB693: fayalite + Qtz in massive Fa-syenite; (c) KB693: fayalite to iddingsite alteration texture; (d) 85BT98: subcalcic augite in massive granite (charnockite); (e) 85BT98: pigeonite in same rock as (d); (f) and (h) KB693: fayalite and cpx overgrown by hastingsite; (h) KB648: fluorite overgrown by hastingsite.

(Fig. 12), the plutonic rocks define a linear array with very high $K_2O + Na_2O$ contents at the low silica end and high $K_2O + Na_2O$ at the high silica end of the array. All fayalite-free granites are silica-rich, Fa-bearing Qtz-syenites and syenites have lower SiO_2 but contain >6 wt % K_2O. The dyke rocks of the Svarthamaren NE wall (Fig. 4) define a different linear array with a marked SiO_2 increase from early to late dykes. The

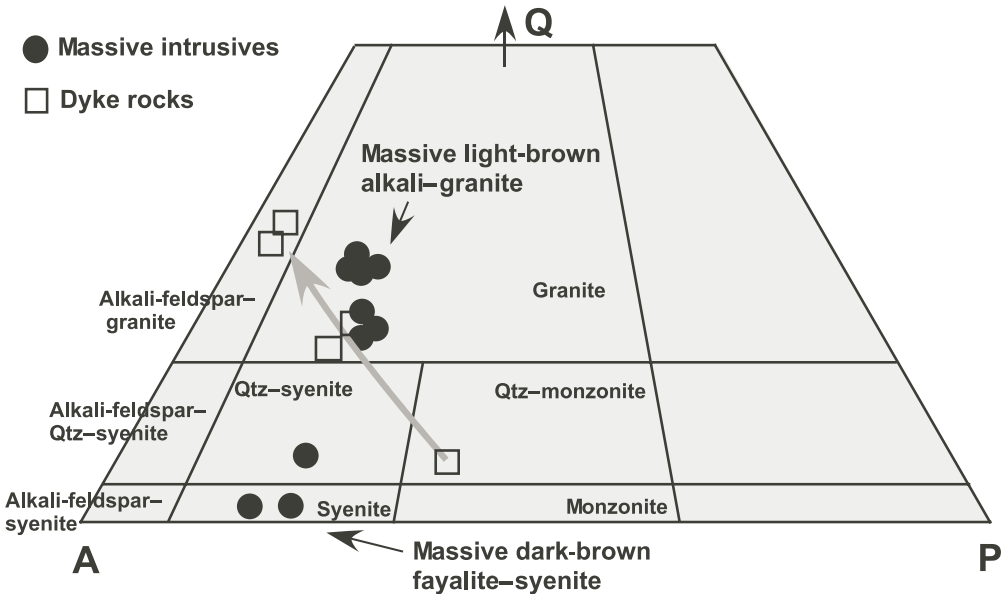

Fig. 10. QAP representation of modal composition data. Light grey arrow represents evolution trend of Svarthamaren dyke rocks.

Table 2: Gneiss xenoliths and country rocks, mineral assemblages, relative abundance and texture data

Rock	Sample	Locality	Qtz	Pl	Kfs	Bt	Opx	Cpx	Grt	Hbl	Other
Mafic and felsic xenoliths	KB623	SK	x	X	x	X	X		X		
	KB627	TN	(x)	X	x	X	X			x	Oam
	KB628	TN	x	X		X	X	X		x	
	KB629	TN	X	X		X	X	X		X	
	KB655	GR	X	X		X	X		X	x	
	KB663	ST	X	X	x	X	X			O	Oam
	KB666b	GR	x	X		X	X		X	x	
	YO14	ST	X	X	x	X			X		
	YO167	PL	X	X	x	X	X				
	YO169	PL	x	X	x	X	X	X			
	BT16	ST	x	X	x	X	X			x	Oam
	BT24	ST	x	X	x	X	X	X	X	x	
	BT95	HS	x	X	x	X	X	X		x	

Rock	Sample	Locality	Qtz	Pl	Kfs	Bt	Opx	Sil	Grt	Crd	Other
Country rocks, metapelite (only)	KB696	HO	X	X	X	X		X	xr	X	
	KB697	HO	X	x	X	X	x		xr	X	
	KB698	HO	X	x	X	X		X	xr	X	Ms
	KB699	HO	X	X	x	X		X	X	X	
	KB700	HO	X	X	x	X			xr	X	
	KB701	HO	X	x	X	X		X	xr	X	
	KB702	HO	X	X	r	X	X	x	X		
	KB703	HO	X	x		X	X	X	x	x	Spl*
	YOEG	MM	X	X	x	X		Ky	X	X	
	YO58B	GR	X	X	x	X			X	X	Spl*

X, major phase; x, minor phase; o, accessory; *as inclusion in Sil, Pl and Crd only; r, relics; HO, SW Hoggestabben; GR, Grjotlia; ST, Stabben; TN, Topograf Nunatak; SK, Skorvetangen; MM, Medmulen; HS, Høgsenga; PL, Plogskaftet; YO and BT samples from Ohta *et al*. (1990).

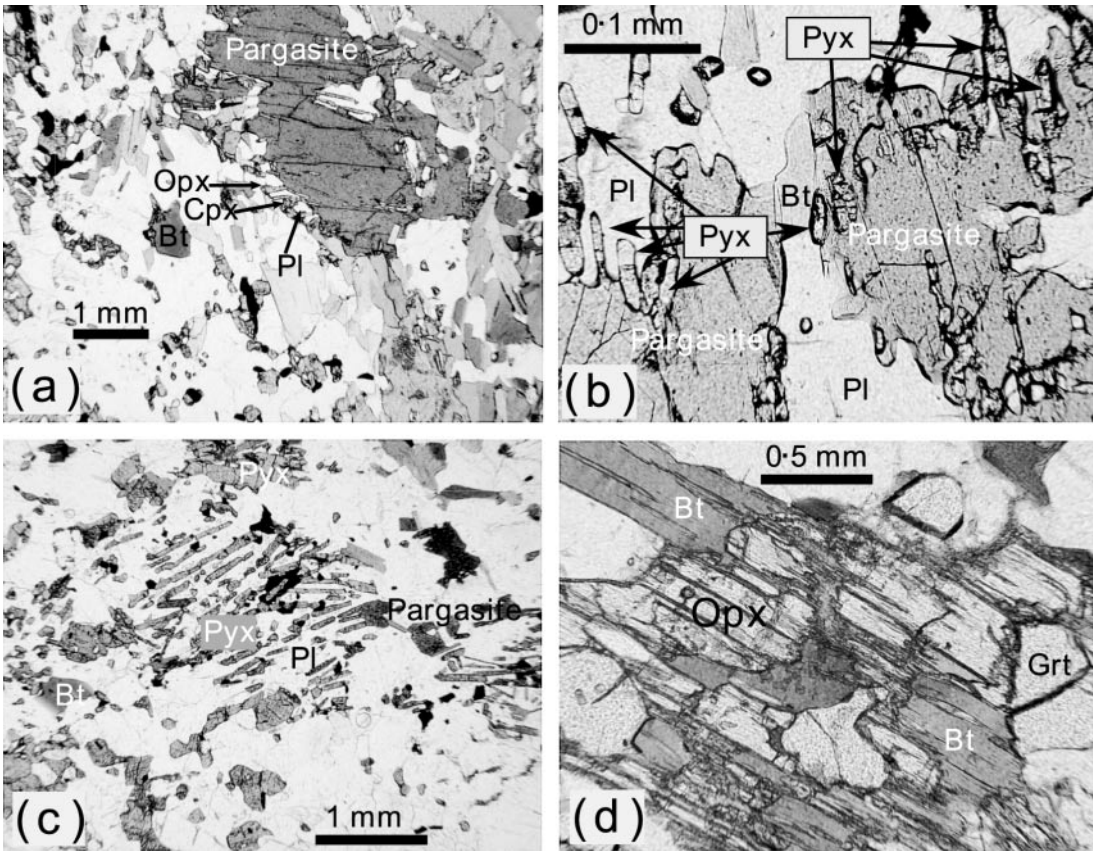

Fig. 11. Photomicrographs of xenoliths: (a) KB628: replacement of pargasitic amphibole by Cpx, Opx and plagioclase along rim; (b) KB628: detail of reaction texture hornblende ⇒ Cpx + Opx + Pl, elongated grains of both types of pyroxene (Pyx) develop together with plagioclase from the decomposition of the amphibole; (c) KB629: pseudomorphic texture of swarms of rod-like pyroxene, with plagioclase after nearly complete dissolution of pargasite; (d) KB623: replacement of orthopyroxene by biotite in Grt–Opx–Kfs-gneiss.

cross-cutting field relationships of the dykes presented earlier show that the observed compositional trend in Fig. 12 corresponds to an evolution of the magma with time. This is indicated by the arrow on the dyke trend in Fig. 12.

The X_{Fe} [$Fe^{2+}/(Fe^{2+} + Mg)$ molar] is about 0·7–0·8 in the alkali-granites and between 0·85 and 0·9 in Fa-syenites. The dyke rocks of the Svarthamaren NE wall show a large variation from 0·55 in the early mafic dyke to >0·95 in the most evolved late alkali-granite dykes. K/Na on a molar basis is between 0·9 and 1·0 for all massive intrusive rocks; dyke rocks are higher (1·55 in KB648). A characteristic feature of anorogenic granites is the high concentration of incompatible trace elements (Fig. 13).

The fluorine and chlorine contents of the alkali-granites are low; the Qtz-syenites also contain relatively small amounts of halogens. All dyke rocks are rich in chlorine; some are unusually rich in fluorine. The light-coloured pink rocks forming halos around gneiss inclusions and bands within the charnockite and Qtz-syenite, however, contain significant amounts of halogens, particularly fluorine.

MINERAL CHEMISTRY

Igneous rocks

Pyroxene

Pigeonite compositions are often difficult to assess as a result of multiple generations of augite exsolution lamellae in a Ca-poor orthopyroxene matrix. Pigeonite in sample 85BT98 was subdivided into three domains: an orthopyroxene matrix, coarse augite exsolution lamellae, and domains with <5 μm mixtures of at least two phases that were analysed with a defocused beam. The three compositions are listed in Table 4, together with a reconstructed pigeonite analysis using modal distribution data that were derived from image analysis of pigeonite in the sample. The wollastonite component in the pigeonite is around 12–13 mol %. Augite is subcalcic with Wo_{35} and X_{Fe} ranging from 0·70 to 0·85. In KB693, hedenbergite contains thin (~5 μm) exsolution lamellae of orthopyroxene. About 1 wt % Al_2O_3 is present as the jadeite component. Orthopyroxene in the fayalite-free rocks is more magnesian than pigeonite.

Table 3: Composition of igneous rocks (major elements, in wt %, trace elements, in ppm)

KB:	602	605	691	704	614	690	705	672	693	694	601	636	638	648	649
SiO_2	75·65	75·76	75·15	74·95	67·74	68·98	66·61	59·51	60·12	61·68	55·43	64·14	67·04	73·86	74·45
TiO_2	0·22	0·25	0·21	0·19	0·37	0·31	0·34	0·81	0·65	0·69	1·86	0·86	0·77	0·33	0·34
Al_2O_3	13·77	14·01	14·09	13·64	14·60	14·91	15·58	16·17	17·36	16·61	14·72	14·12	13·96	11·88	11·53
Fe_2O_3	0·46	0·84	0·27	0·57	1·55	0·89	1·06	2·20	1·93	1·40	1·71	1·84	1·22	1·82	1·63
FeO	1·32	1·01	1·39	1·34	1·99	1·98	2·58	5·23	3·87	3·68	5·73	4·18	3·82	2·18	2·44
MnO	0·02	0·03	0·03	0·04	0·05	0·06	0·08	0·17	0·13	0·07	0·09	0·07	0·06	0·05	0·04
CaO	1·30	1·31	1·18	1·11	1·94	1·45	1·50	3·23	2·68	2·27	4·67	2·96	2·64	1·57	1·49
MgO	0·26	0·22	0·23	0·19	0·15	0·23	0·16	0·43	0·35	0·66	2·61	0·67	0·54	0·06	0·07
Na_2O	3·49	3·44	3·83	3·92	3·33	4·14	4·36	4·25	4·51	4·19	3·39	2·85	3·06	2·46	2·38
K_2O	5·15	5·41	5·20	5·27	5·93	5·80	6·36	6·83	6·72	6·42	4·58	5·39	5·19	5·86	5·61
P_2O_5	0·05	0·05	0·05	0·05	0·08	0·06	0·04	0·16	0·11	0·23	1·15	0·21	0·24	0·05	0·06
LOI	0·20	0·12	0·20	0·98	0·54	0·19	0·07		0·01	0·14	0·11	0·18	0·30	0·58	1·02
Total	101·89	102·45	101·83	102·25	98·27	99·00	98·74	98·99	98·44	98·04	96·05	97·47	98·84	100·70	101·06
Ba	644	1026	640	445	3483	548	574	1215	1026	2349	5410	2983	2836	337	393
Pb	40	46	56	48	50	51	44	36	43	42	47	42	40	63	63
Rb	190	197	248	140	125	170	106	86	100	143	112	129	129	187	175
Sc	6	5	2	5	6	4	5	14	10	9	10	13	8	4	6
Sr	151	175	169	97	488	138	137	181	219	374	1845	427	432	65	70
V	18	21	19	13	18	22	13	31	26	35	148	48	45	14	11
Zn	57	59	34	84	92	64	47	148	105	95	132	133	116	142	148
Zr	178	226	194	729	662	497	176	522	807	629	317	1033	680	682	710
C	627	615	633	532	527	558	654	478	546	586	548	547	584	618	608
Ce	47	48	48	51	53	50	46	69	62	66	106	72	70	50	51
Cl	75	68	72	198	134	79	55	63	2	184	355	407	409	373	355
F	364	175	1010	571	200	753	181	106	20	1534	3158	1857	2581	6000	3721
Hf	6	5	6	13	13	13	7	15	13	12	4	22	14	19	18
La	51	74	84	323	143	214	61	50	86	115	283	274	190	634	569
Mo	2	6	13	9	6	7	3	5	5	6	4	7	7	10	9
Nb	12	12	13	31	22	29	19	42	23	23	15	41	26	40	44
Th	15	12	18	10	9	26	14	10	10	8	5	17	11	10	8
Y	34	38	44	49	40	43	28	36	24	50	37	89	62	109	113
S											127	875			

Olivine

Olivine is close to fayalite end-member composition (Fa_{96}). MnO is typically higher than MgO, and CaO is very low. In dyke sample KB648, pure stoichiometric fayalite has been found with only traces of other components ($X_{Fe} > 0{\cdot}999$).

Feldspar

Compositions of host and lamellae of mesoperthite in KB693 are given in Table 5, together with modal proportions of host and lamellae analysed with image analysis. The reconstructed alkali feldspar composition is about Or_{64} with a very low anorthite component. The alkali feldspars are essentially binary Ab–Or feldspars. Plagioclase is typically oligoclase ($An_{10–20}$). No compositional features are present that permit the distinction of plagioclase of primary versus exsolution origin.

Amphibole

Unzoned ferro-hastingsite is the primary amphibole present in all the analysed igneous rocks (Table 6). Amphibole has a very similar composition in brown and pink variety granites. The amphiboles are unzoned. The amphibole is rich in potassium (0·24–0·40 K pfu). The two dyke rocks contain hastingsite with a high F (0·35 F pfu) and Cl content. The rocks also contain

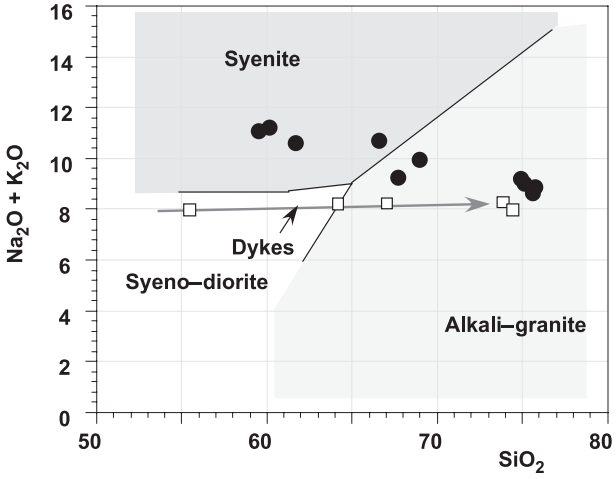

Fig. 12. $Na_2O + K_2O$ vs SiO_2 diagram. Massive plutons black circles, dyke rocks open squares. Light grey arrow represents evolution trend of Svarthamaren dyke rocks.

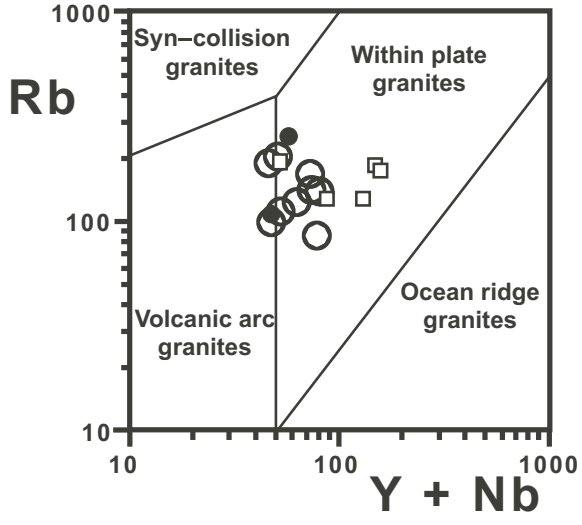

Fig. 13. Rb vs Y+Nb granitoid discrimination diagram after Pearce *et al.* (1984). Symbols as in Fig. 12.

igneous fluorite and F-apatite. The stoichiometry of all hastingsites requires a high proportion of oxy-hastingsite component.

Biotite

Biotite has a very similar composition in both brown and pink granites, and is extremely Fe-rich (Mg-poor) in these rocks (Table 7). X_{Fe} of 0·7–0·8 is typical in Fa-syenite; in the late dykes, $X_{Fe} = 0·95$. In the massive plutonic rocks, biotite is F-rich. Biotite of the two late dykes contains slightly less F but a high content of Cl. An additional observation is that biotite contains no octahedral Al. The stoichiometry further suggests the presence of Fe^{3+}.

Accessory minerals

Fluorite was identified in the two dyke samples: KB648 and KB649. Stoichiometric pure fluorapatite $Ca_5(PO_4)_3F$ is present in the two dyke samples, KB648 and KB649, and in Qtz-syenite, KB693. Cerium-rich allanite in the two dyke samples, KB648 and KB649, also contains La, Sm and Nd. Magnetite and ilmenite were identified in all microprobe sections. Their compositions are variable and their textures suggest disequilibrium (see petrography above).

Xenoliths and country rocks

The composition of minerals in the metapelitic gneisses was presented by Bucher-Nurminen & Ohta (1993). Pyroxene analyses from mafic gneiss xenoliths are given in Table 8. Orthopyroxene is generally low in Al content and X_{Fe} varies from 0·62 to 0·75. Clinopyroxene contains more Al and lower X_{Fe} than coexisting orthopyroxene. About half of the Al is tied to the jadeite component and the remainder to the Tschermak component. The amount of the Tschermak component in the two pyroxenes is similar. The analyses from samples KB628 and KB629 characterize coexisting Opx and Cpx produced by the decomposition of amphibole in the samples as indicated by the textures (Fig. 11). Mafic gneiss samples contain plagioclase with 35–40 mol % anorthite component (Table 9). The decomposing amphibole (Fig. 11) in the gneiss xenoliths is a ferropargasite in clear contrast to the hastingsite of the igneous rocks (Table 10). It contains about 1 wt % fluorine and 0·2 wt % chlorine. A small amount of total iron is probably present as Fe^{3+}, in contrast to the pyroxenes. This, in turn, may suggest that the amphibole decomposition reaction involves a redox component. Garnet is weakly zoned with iron-rich cores and Mg-rich rims (Table 11). It contains similar amounts of Mg and Ca. Biotite contains high amounts of titanium and more than 2 wt % of fluorine (Table 12).

THERMOBAROMETRY

The igneous rocks

The ferromagnesian assemblages of the granitoids depend on the X_{Fe} of the bulk-rock. Those rocks with the highest X_{Fe} have the assemblage hedenbergite (or subcalcic augite)–fayalite, whereas more magnesian rocks contain pigeonite + augite. The three-phase assemblage pigeonite–augite–olivine (+ Qtz) was not observed in the studied samples (Fig. 14). These assemblages can place constraints on the temperature and pressure of crystallization.

The most useful sample for estimation of temperature is 85BT98, which contains augite and pigeonite. This

Table 4: Pyroxene and olivine analyses

Sample:	85BT98					90YOA18		KB693		
	1	2	3	Pigeonite	Augite	Pigeonite	Augite	Augite*[1]	Augite** 2	Olivine
Mode %:	55·66	8·19	36·15	recons.	recons.	recons.				
SiO_2	49·44	49·71	49·07	49·33	49·70	48·80	49·62	50·87	49·95	29·36
TiO_2	0·15	0·31	0·17	0·17	0·30	0·11	0·16	0·20	0·14	
Al_2O_3	0·40	1·16	0·48	0·49	1·04	0·50	0·99	0·82	0·89	
FeO	43·63	25·54	39·34	40·60	28·34	37·89	25·02	26·11	29·60	67·33
MnO	0·63	0·31	0·64	0·61	0·40	0·64	0·37	0·86	0·89	1·79
MgO	4·54	3·93	4·61	4·52	4·11	6·03	5·45	3·05	3·00	1·53
CaO	2·55	17·08	6·14	5·04	15·36	5·77	17·26	18·35	14·87	0·03
Na_2O	0·04	0·29	0·10	0·08	0·27	0·09	0·30	0·41	0·35	
K_2O	0·01		0·01	0·01	0·01	0·01	0·01	0·01	0·04	
Total	101·39	98·33	100·56	100·84	99·53	99·85	99·17	100·67	99·73	100·01
Si	2·047	2·042	2·028	2·040	2·028	2·013	2·004	2·052	2·052	0·988
Ti	0·005	0·01	0·005	0·005	0·009	0·004	0·005	0·006	0·004	
Al	0·020	0·056	0·023	0·024	0·050	0·024	0·047	0·039	0·043	
Fe	1·511	0·877	1·360	1·404	0·967	1·307	0·845	0·881	1·017	1·895
Mn	0·022	0·011	0·022	0·021	0·014	0·022	0·013	0·029	0·031	0·051
Mg	0·280	0·241	0·284	0·278	0·250	0·371	0·328	0·183	0·184	0·077
Ca	0·113	0·752	0·272	0·223	0·671	0·255	0·747	0·793	0·654	0·001
X_{Fe}	0·844	0·785	0·827	0·834	0·795	0·779	0·720	0·828	0·847	0·96
En	14·72	12·87	14·83	14·61	13·24	19·19	17·08	9·88	9·90	
Fs	79·34	46·92	70·98	73·67	51·20	67·61	44·01	47·42	54·81	
Wo	5·94	40·20	14·19	11·71	35·56	13·19	38·91	42·70	35·28	

Textures (see Fig. 7): 1, Opx matrix; 2, augite exsolution; 3, finely exsolved domains analysed with defocused beam; *analysed with defocused beam; **subcalcic augite; [1]granular exsolved augite; recons., reconstructed composition.

assemblage contains three thermometers (Frost & Lindsley, 1992; Lindsley & Frost, 1992): (1) the composition of pigeonite (assuming it is saturated with respect to augite); (2) the composition of augite (as saturated with pigeonite); (3) the Fe–Mg distribution between augite and pigeonite. The last is not a very robust thermometer, but all three thermometers must give the same result for an equilibrium assemblage. Using the compositions in Table 4, the QUILF program of Andersen *et al.* (1993) gives a temperature of 898 ± 97°C. The large uncertainty stems from the fact that the two pyroxenes are not quite in Fe–Mg exchange equilibrium. This can be seen by calculating the augite composition in equilibrium with the composition of the reconstructed pigeonite, and, vice versa, calculating the pigeonite composition in equilibrium with average augite (Fig. 15). Equilibrium augite would be more Fe-rich and lower in Ca than the analysed augite, whereas pigeonite in equilibrium with the analysed augite would be more Mg-rich and have lower Ca than the reconstructed pigeonite. We consider that part of this uncertainty is a result of Fe–Mg exchange on cooling, and part may be a result of the fact that our reconstitution of the highly exsolved pigeonite may have slightly overestimated its Ca content. We regard 900°C (± 25°C) as the best estimate for the crystallization of the pyroxene pairs in 85BT98. Because the mafic minerals are texturally younger than the feldspar and quartz, the temperature of 900°C is considered to represent the solidus temperature.

The assemblage in 85BT98 also provides an estimate of the minimum pressure for the conditions of magma crystallization. This can be obtained by calculating the pressure at which olivine would appear in the assemblage augite–pigeonite–Qtz using the QUILF software (Andersen *et al.*, 1993). At 900°C, this pressure is 360 MPa. At pressures of <360 MPa, olivine would have been stable in this rock instead of pigeonite. The maximum pressure can be obtained from Fa-syenite sample KB693, which contains olivine + augite + Qtz but lacks pigeonite. One could use the temperature calculated from 85BT98, but the augite in KB693 is relatively Ca-rich and is distinct from the calculated augite

Table 5: Feldspar analyses

Samples:	KB648		KB649		KB694		KB693				KB705	
	Kfs	Pl	Kfs	Pl	Kfs	Pl	Msp* Host	Msp* lamellae	Msp* recons.	Pl	Kfs	Pl
Mode %:							73	27				
SiO_2	65·79	62·13	65·29	63·39	65·00	63·17	64·96	69·95	66·30	65·17	66·60	66·01
Al_2O_3	19·35	23·37	19·64	24·15	19·48	23·83	17·41	18·80	17·78	21·32	19·56	22·24
FeO	0·02	0·06	0·07	0·07	0·02	0·06	0·43	0·09	0·34	0·15	0·01	0·01
CaO	0·06	4·81	0·12	4·30	0·13	4·06	0·05	0·18	0·08	3·67	0·42	2·37
Na_2O	3·52	9·61	2·97	8·86	3·82	8·72	1·39	11·26	4·03	9·47	4·38	10·35
K_2O	11·34	0·23	10·96	0·17	10·96	0·25	15·02	0·11	11·03	0·23	10·31	0·30
Total	100·09	100·23	99·08	100·95	99·47	100·11	98·83	100·30	99·22	100·01	101·26	101·276
Si	2·991	2·729	3·01	2·782	2·967	2·798	3·015	3·059	3·027	2·884	2·980	2·865
Al	1·037	1·210	1·07	1·249	1·048	1·244	0·952	0·969	0·957	1·112	1·031	1·137
Fe	0·001	0·002	0·00	0·003	0·001	0·002	0·017	0·003	0·013	0·006	0·0	0·0
Ca	0·003	0·226	0·01	0·202	0·006	0·193	0·002	0·008	0·004	0·174	0·020	0·110
Na	0·310	0·818	0·26	0·754	0·338	0·749	0·125	0·954	0·357	0·812	0·380	0·871
K	0·658	0·013	0·65	0·01	0·638	0·014	0·889	0·006	0·643	0·013	0·588	0·017
X_{Or}	0·68	0·01	0·70	0·01	0·65	0·01	0·87	0·01	0·64	0·01	0·60	0·017
X_{An}	0·00	0·21	0·01	0·21	0·01	0·20	0·01	0·01	0·01	0·17	0·01	0·11

Msp*, mesoperthite; cations (O = 8).

composition for this rock at 900°C. To obtain the maximum pressure, therefore, we calculated the pressure and temperature (540 MPa, 798°C) at which the olivine in KB693 would be in equilibrium with pigeonite, orthopyroxene and augite (Fig. 16). This is the low-temperature limit for pigeonite in rocks of this composition and the coexistence of augite, pigeonite and opx fixes the Ca-content of the pyroxenes. Interestingly, the augite analysed by a broad beam from KB693 has nearly the composition of augite that would be in equilibrium, indicating that it had re-equilibrated down to temperatures of around 800°C. A minimum solvus temperature of 714°C based on albite in alkali feldspar and plagioclase can be calculated from reconstructed mesoperthite compositions (Fuhrman & Lindsley, 1988; Kroll *et al.*, 1993).

Xenoliths and country rock gneisses

The intrusion of the Palaeozoic plutons pervasively overprinted gneisses and metasedimentary country rocks. The detailed thermal structure of the contact aureoles has not been studied. However, biotite–garnet–cordierite–sillimanite assemblages in metapelites about 100 m from the contact with the Qtz-syenite pluton (locality 'A', Fig. 2) indicate about 700°C at 400 MPa (Bucher-Nurminen & Ohta, 1993). The thermobarometric analysis and the composition of cordierite indicate the presence of CO_2 during reaction and equilibration (Bucher-Nurminen & Ohta, 1993) and an activity of H_2O of 0·7–0·8 (standard state: $aH_2O = 1$ for pure phase component at P and T). At locality 'B' (Fig. 2), about 600 m from the intrusive contact similar mineral assemblages yielded 650°C at the same pressure and water activity. Calc-silicate rocks and Grs–Di-marbles occurring in the metasedimentary gneiss sequence at both localities are a potential source for the CO_2 in the fluid. Wollastonite marbles occur at two localities close to the contact with the pluton. The formation of wollastonite requires aCO_2 less than 0·2 at 650°C and less than 0·4 at 700°C at 400 MPa.

The garnet–orthopyroxene–clinopyroxene–plagioclase–amphibole assemblages of the gneissic xenoliths in the granitoid rocks record temperatures of 750–800°C at the same pressure of 400 MPa, and aH_2O estimates range from 0·8 to 0·5. Thermobarometry data were computed from the program GTB (Spear & Kohn, 1999) using the mineral composition data for three samples (Tables 8–12). The following equilibria have been utilized: Grt–Bt Fe–Mg exchange (Ferry & Spear, 1978; Grt solution model: Berman, 1990): Grt–Hbl Fe–Mg exchange (Perchuk *et al.*, 1985): Hbl–Pl (Holland & Blundy, 1994): Grt–Pl–Hbl–Qtz (Kohn & Spear, 1989). TWEEQU (Thermobarometry With Estimation of EQUilibrium state; Berman, 1991), which involves calculation of all

Table 6: Hastingsite analyses

Sample:	KB648*	KB649*	KB693	KB694
SiO_2	36·55	36·84	39·91	39·85
TiO_2	1·09	1·22	1·75	1·63
Al_2O_3	10·57	10·87	9·08	9·55
Fe_2O_3	8·01	8·03	8·09	7·59
FeO	25·55	25·63	23·07	21·63
MnO	0·28	0·32	0·38	0·51
MgO	0·55	0·60	2·47	3·69
CaO	10·00	10·02	10·24	10·35
Na_2O	1·85	1·80	1·66	1·86
K_2O	1·88	1·81	1·16	1·35
F	0·64	0·68	0·25	0·77
Cl	1·37	1·07	0·05	0·27
H_2O	1·24	1·20	1·70	1·45
Total	99·59	100·10	99·82	100·53
O = F	0·27	0·29	0·10	0·32
O = Cl	0·31	0·24	0·01	0·06
Real total	99·01	99·57	99·71	100·15
FeO measured	32·76	32·86	30·35	28·47
Si	6·05	6·05	6·37	6·30
Al IV	1·95	1·95	1·63	1·70
Al VI	0·12	0·16	0·08	0·09
Ti	0·14	0·15	0·21	0·19
Fe^3	1·00	0·99	0·97	0·90
Fe	3·54	3·52	3·08	2·86
Mn	0·04	0·04	0·05	0·07
Mg	0·14	0·15	0·59	0·87
Ca	1·77	1·76	1·75	1·75
Na	0·59	0·57	0·51	0·57
K	0·40	0·38	0·24	0·27
F	0·34	0·35	0·13	0·39
Cl	0·39	0·30	0·01	0·07
O	0·31	0·49	0·43	0·35
OH	1·06	0·82	1·38	1·18
X_{Fe}	0·96	0·96	0·84	0·77
X_K	0·40	0·40	0·31	0·32

Fe^3/Fe^2 estimate and H_2O based on stoichiometry; *dyke rocks; cations recalculated on the basis of 24 O.

Table 7: Biotite analyses

Sample:	KB848 a	KB848 b	KB649	KB694
SiO_2	32·84	32·73	33·06	34·28
TiO_2	3·29	3·93	4·65	3·99
Al_2O_3	12·73	12·63	12·51	12·77
Fe_2O_3	1·99	1·98	0·39	0·33
FeO	34·09	33·83	34·51	29·74
MnO	0·17	0·20	0·27	0·20
MgO	1·22	0·87	0·94	4·99
Na_2O	0·04	0·06	0·05	0·07
K_2O	8·79	8·73	8·49	8·92
F	1·11	0·95	0·87	1·44
Cl	0·70	1·00	1·12	0·27
H_2O	2·85	2·85	2·85	2·90
Total	99·84	99·77	99·71	99·96
O = F	0·47	0·40	0·37	0·61
O = Cl	0·16	0·23	0·25	0·06
Rec total	99·21	99·14	99·09	99·29
FeO meas.	35·88	35·61	34·86	30·04
Si	5·50	5·49	5·53	5·56
Al IV	2·50	2·51	2·47	2·44
Al VI	0·01	0·00	0·00	0·00
Ti	0·41	0·50	0·59	0·49
Fe^3	0·25	0·25	0·05	0·04
Fe	4·77	4·74	4·83	4·03
Mn	0·02	0·03	0·04	0·03
Mg	0·30	0·22	0·23	1·21
Na	0·01	0·02	0·02	0·02
K	1·88	1·87	1·81	1·85
F	0·59	0·50	0·46	0·74
Cl	0·20	0·28	0·32	0·07
OH	3·18	3·19	3·18	3·14
X_{Fe}	0·94	0·96	0·95	0·77

Fe^3/Fe^2 estimate and H_2O based on stoichiometry; a, early Bt; b, late Bt; cations recalculated on the basis of 24 O.

possible equilibria implied by a given mineral assemblage, provided a second set of P–T data. The thermodynamic data of all phase components, including H_2O, were taken from Holland & Powell (1990). The thermodynamic properties of the solid-solution were modeled for garnet using the formulation of Berman (1990), for plagioclase that of Fuhrman & Lindsley (1988), and all other solutions were modelled as ideal solutions. The standard state is defined as a pure phase component at P and T. The simultaneous solution of about 60 equilibria revealed a mean temperature of 770°C and a mean pressure of 380 MPa. Both methods indicate 780 ± 20°C and 400 ± 20 MPa for the gneiss assemblage Grt–Bt–Hbl–Opx–Cpx–Pl–Qtz and reflect the P–T conditions of contact metamorphism caused by the Palaeozoic intrusives.

REACTIONS AND EQUILIBRIA

Reactions in the igneous rocks

The key assemblage of the high-T igneous rocks is feldspar–olivine–augite–pigeonite–hastingsite–Qtz. This solid phase assemblage coexisted with a silicate melt phase above the solidus. The textures suggest that the

Table 8: Pyroxene from gneiss xenoliths

Sample:	628	628	628	628	629	629	629	629	629	623	623
Spot:	opx6	opx7	cpx6	cpx10	opx1	opx2	opx3	cpx1	cpx3	opx5	opx6
SiO_2	48·33	48·56	50·28	50·57	47·87	49·22	48·44	49·37	50·38	48·62	48·61
TiO_2	0·13	0·09	0·18	0·15	0·10	0·09	0·10	0·30	0·18	0·07	0·08
Al_2O_3	0·32	0·32	0·99	0·76	0·37	0·32	0·40	1·12	1·05	1·12	1·08
FeO*	39·32	39·74	18·51	18·20	42·90	37·99	40·15	21·77	19·25	36·78	36·64
MnO	1·06	1·01	0·46	0·45	0·89	1·42	1·01	0·47	0·50	0·52	0·56
MgO	10·36	9·79	8·12	8·40	8·03	11·21	9·35	6·93	7·95	12·71	12·74
CaO	0·84	0·88	20·93	21·50	0·67	0·71	1·06	19·62	20·47	0·30	0·32
Na_2O	0·01	0·01	0·30	0·29	0·02	0·02	0·00	0·26	0·23	0·01	0·02
Total	100·38	100·41	99·77	100·32	100·85	100·98	100·52	99·84	100·01	100·14	100·06
Si	1·965	1·976	1·968	1·968	1·969	1·974	1·974	1·957	1·970	1·947	1·948
Ti	0·004	0·003	0·005	0·004	0·003	0·003	0·003	0·009	0·005	0·002	0·002
Al	0·015	0·015	0·046	0·035	0·018	0·015	0·019	0·052	0·048	0·053	0·051
Fe	1·337	1·352	0·606	0·592	1·476	1·274	1·368	0·722	0·630	1·232	1·228
Mn	0·037	0·035	0·015	0·015	0·031	0·048	0·035	0·016	0·017	0·018	0·019
Mg	0·628	0·594	0·474	0·487	0·492	0·670	0·568	0·410	0·464	0·759	0·761
Ca	0·037	0·038	0·878	0·897	0·030	0·031	0·046	0·833	0·858	0·013	0·014
Na	0·001	0·001	0·023	0·022	0·002	0·002	0·000	0·020	0·017	0·001	0·002
X_{Fe}	0·68	0·69	0·56	0·55	0·75	0·66	0·71	0·64	0·58	0·62	0·62

*All Fe as Fe^{2+}; cations based on 6 O.

Table 9: Feldspar from gneiss xenoliths in fayalite-syenite and charnockite

	Plagioclase										K-feldspar		
Sample:	628	628	628	628	629	629	623	623	623	623	628	628	629
Spot:	pl4	pl5	pl7	pl7	pl1	pl2	pl1	pl2	pl3	pl4	kfs4	kfs4	kfs1
SiO_2	59·56	59·64	59·25	60·85	57·97	56·87	58·87	59·59	59·24	58·73	64·56	65·60	64·60
Al_2O_3	26·15	26·01	25·87	25·22	26·95	27·37	27·37	27·29	26·96	27·07	19·31	19·39	19·36
FeO	0·28	0·31	0·32	0·11	0·05	0·13	0·01	0·06	0·28	0·06	0·02	0·08	0·01
CaO	7·19	6·99	7·16	6·33	8·32	8·81	8·15	7·81	7·65	7·94	0·02	0·00	0·06
Na_2O	7·33	7·40	7·32	7·72	6·81	6·45	6·50	6·80	6·42	6·60	1·01	1·32	1·18
K_2O	0·27	0·37	0·36	0·35	0·10	0·14	0·16	0·17	0·18	0·20	14·49	13·68	14·26
Total	100·79	100·74	100·33	100·61	100·21	99·77	101·06	101·74	100·84	100·60	99·45	100·15	99·52
Si	2·638	2·642	2·637	2·695	2·587	2·554	2·613	2·623	2·639	2·616	2·994	3·021	2·991
Al	1·365	1·358	1·356	1·316	1·417	1·448	1·431	1·416	1·415	1·421	1·055	1·052	1·056
Fe	0·010	0·011	0·012	0·004	0·002	0·005	0·000	0·002	0·010	0·002	0·001	0·003	0·000
Ca	0·341	0·332	0·341	0·300	0·398	0·424	0·388	0·368	0·365	0·379	0·001	0·000	0·003
Na	0·629	0·635	0·631	0·663	0·589	0·561	0·559	0·580	0·554	0·570	0·091	0·118	0·106
K	0·015	0·021	0·020	0·020	0·006	0·008	0·009	0·010	0·010	0·011	0·857	0·804	0·842
An	0·35	0·34	0·34	0·31	0·40	0·43	0·41	0·38	0·39	0·39	0·00	0·00	0·00
Ab	0·64	0·64	0·64	0·67	0·59	0·57	0·59	0·61	0·60	0·59	0·10	0·13	0·11
Or	0·02	0·02	0·02	0·02	0·01	0·01	0·01	0·01	0·01	0·01	0·90	0·87	0·89

Cations based on 8 O.

Table 10: Amphibole from xenoliths

Sample:	KB628*	KB629
SiO_2	42·42	42·16
TiO_2	1·62	1·89
Al_2O_3	9·78	10·25
FeO**	22·06	19·86
MnO	0·22	0·26
MgO	7·81	8·83
CaO	11·02	11·15
Na_2O	1·37	1·53
K_2O	1·57	1·55
F	0·82	1·21
Cl	0·25	0·13
Total***	98·94	98·82
Si	6·453	6·398
Al	1·754	1·834
Ti	0·185	0·216
Fe	2·807	2·521
Mn	0·028	0·033
Mg	1·771	1·998
Ca	1·796	1·813
Na	0·404	0·450
K	0·305	0·300
F	0·395	0·581
Cl	0·065	0·033
X_{Fe}	0·613	0·558

Stoichiometry based on cations−Ca−Na−K = 13; *average of about 10 spot analyses per sample; **all Fe as FeO; ***uncorr. for halogens.

Table 11: Garnet from xenolith sample KB623

Spot #	grt1	grt2	grt3	grt3
SiO_2	37·20	37·39	36·97	36·98
Al_2O_3	21·38	21·24	21·16	21·18
FeO*	35·49	35·17	35·52	35·65
MnO	1·73	1·75	1·82	1·85
MgO	3·22	3·15	3·00	2·45
CaO	2·68	2·74	2·92	3·28
Total	101·70	101·44	101·39	101·39
Si	2·955	2·974	2·953	2·958
Al	2·003	1·991	1·993	1·997
Fe	2·358	2·339	2·373	2·385
Mn	0·116	0·118	0·123	0·125
Mg	0·381	0·374	0·357	0·292
Ca	0·228	0·233	0·250	0·281
X_{Fe}	0·86	0·86	0·87	0·89
Alm	78·60	77·98	79·11	79·49
Sps	3·88	3·93	4·10	4·18
Prp	12·71	12·45	11·91	9·74
Grs	7·60	7·78	8·33	9·37

*All Fe as Fe^{2+}; stoichiometry based on 12 O.

minerals represent an igneous equilibrium assemblage. This requires equilibrium of reaction (1) among the phase components:

$$6CaFeSi_2O_6 + 7Fe_2SiO_4 + 2CaAl_2Si_2O_8 + 4NaAlSi_3O_8 + O_2 + 4H_2O = 4NaCa_2Fe_4Fe_1Al_2Si_6O_{22}(OH)_2 + 11SiO_2. \quad (1)$$

Quantitative calculation of the equilibrium conditions of reaction (1) is not possible because thermodynamic data for hastingsite are lacking. However, this redox reaction converts Hd + Fa + Pl to hastingsite if aO_2 or aH_2O increase. Hastingsite in sample KB693 is compositionally collinear with hedenbergite and fayalite on the pyroxene projection (Fig. 14) as a consequence of reaction (1). Because reaction (1) at or above the solidus involves a melt phase in addition to the solid phases, the volatile components are phase components of the melt phase. If aH_2O is low, the system may not be saturated with a low-density fluid phase and the volatile components are dissolved in the melt phase alone.

Hastingsite also contains halogens; therefore, equation (1) can be written with HF instead of H_2O as a reactant:

$$6CaFeSi_2O_6 + 7Fe_2SiO_4 + 2CaAl_2Si_2O_8 + 4NaAlSi_3O_8 + O_2 + 8HF = 4NaCa_2Fe_4Fe_1Al_2Si_6O_{22}(OH)_2 + 11SiO_2 + 4H_2O. \quad (2)$$

The introduction of HF (or HCl) has the interesting consequence that amphibole formation produces rather than consumes H_2O. The overall consequences of halogen-components for the H_2O budget at the solidus could be substantial; however, it cannot be assessed quantitatively because most rocks (except for the most evolved dykes) are not saturated with solid halogenides.

In the two dyke rocks (KB648 and KB649), hedenbergite is lacking. This may indicate that reaction (1) went to completion and fO_2 in the dyke rocks was higher than in the massive charnockite. In addition, the dyke rocks contain late igneous fluorite, which probably formed from the reaction

$$2CaFeSi_2O_6 + 4HF = 2CaF_2 + Fe_2SiO_4 + 3SiO_2 + 2H_2O. \quad (3)$$

Reaction (3) consumes pyroxene and converts it into fluorite and fayalite. Combining reactions (1) and (3) results in a hedenbergite-absent reaction for the dyke

Table 12: Biotite from gneiss xenoliths

Sample:	KB628[1]	KB629	KB623
SiO_2	36·73	36·74	35·00
TiO_2	4·10	4·25	3·93
Al_2O_3	12·99	12·99	15·16
FeO*	22·37	20·03	23·56
MnO	0·09	0·11	0·10
MgO	10·32	12·00	9·17
CaO	0·01	0·01	0·03
Na_2O	0·04	0·11	0·07
K_2O	9·21	8·94	8·87
F	1·90	2·59	0·44
Cl	0·26	0·09	0·07
$H_2O^{\dagger}$	2·90	2·90	3·60
Total	100·95	100·77	100·00
O = F	0·80	1·09	0·19
O = Cl	0·06	0·02	0·02
Real total	100·09	99·66	99·80
Si	5·664	5·607	5·429
Al^{IV}	2·336	2·393	2·571
Al^{VI}	0·025	−0·056	0·202
Ti	0·475	0·488	0·458
Fe*	2·885	2·556	3·057
Mn	0·012	0·014	0·013
Mg	2·373	2·731	2·121
Ca	0·002	0·002	0·005
Na	0·012	0·033	0·021
K	1·812	1·741	1·755
F	0·927	1·250	0·216
Cl	0·068	0·023	0·018
OH	2·986	2·955	3·729
$X_{Fe^{2+}}$	0·549	0·484	0·590

[1]Average of about 10 spot analyses per sample; *all Fe as Fe^{2+}; [†]H_2O based on stoichiometry; stoichiometry based on 24 O.

rocks:

$$6CaF_2 + 10Fe_2SiO_4 + 2CaAl_2Si_2O_8 + 4NaAlSi_3O_8 + O_2 + 10H_2O = 4NaCa_2Fe_4Fe_1Al_2Si_6O_{22}(OH)_2 + 2SiO_2 + 12HF. \quad (4)$$

From equation (4), it is evident that the solid phases in the dyke rocks cannot control the activities of the volatile phase components. Furthermore, the magma of the dyke rocks cannot evolve simultaneously to both higher fO_2 and higher fHF conditions because of the inverse O_2–HF relationship in equation (4). This holds true also if equation (4) is written with F-hastingsite as a phase component of the amphibole. We suggest that igneous fluorite was first produced by reaction (3) and then, after all pyroxene was consumed, hastingsite formed by reaction (4).

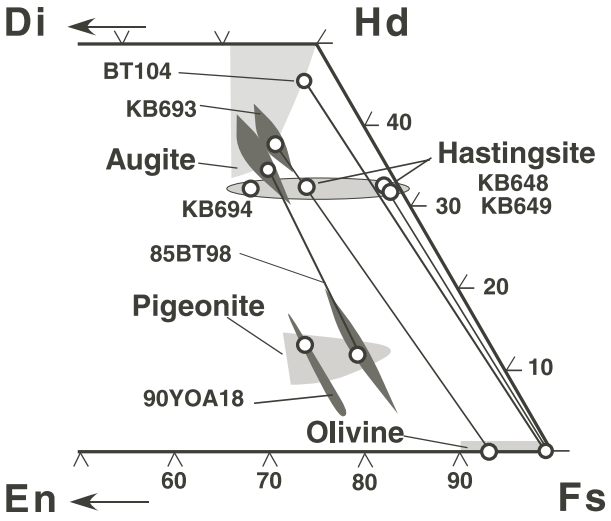

Fig. 14. Pyroxene quadrilateral showing the phase relations of charnockite and Qtz-syenite samples. Light shading: one-phase fields for pigeonite and augite at the estimated conditions of charnockite formation. Dark shading: field containing all single spot microprobe data for the mineral with the average composition represented with an open circle. Hastingsite compositions are projected onto the quadrilateral from quartz, feldspar and fluid.

Redox conditions

The assemblage Hd–Fa–Pl–Qtz–hastingsite is capable of buffering O_2 via equilibrium (1) at a given aH_2O. Although a quantitative estimate of fO_2 from equilibrium (1) cannot be given, the presence of fayalite + Qtz requires fO_2 conditions low enough to prevent conversion to magnetite according to the reaction

$$3Fe_2SiO_4 + O_2 = 2Fe_3O_4 + 3SiO_2. \quad (5)$$

Consequently, the Fa + Qtz assemblage requires log fO_2 below that of the QFM buffer. Defining $\Delta\log fO_2$ as $[\log fO_{2\ \text{assemblage}} - \log fO_{2\ \text{QFM}}]$, it follows that $\Delta\log fO_2 < 0$ for all aH_2O conditions at, or above, the solidus. Some rock samples show textural evidence of late retrogression alteration, and magnetite rinds around fayalite and magnetite in iddingsite textures indicate progress of reaction (5). At solidus conditions, all rocks formed under $\Delta\log fO_2 < 0$ [fO_2 below that defined by equilibrium (5)].

As magnetite is a subsolidus phase in all rocks, a further limit to the redox conditions can be deduced from the coexistence of biotite and K-feldspar:

$$2KFe_3AlSi_3O_{10}(OH)_2 + O_2 = 2KAlSi_3O_8 + 2Fe_3O_4 + 2H_2O. \quad (6)$$

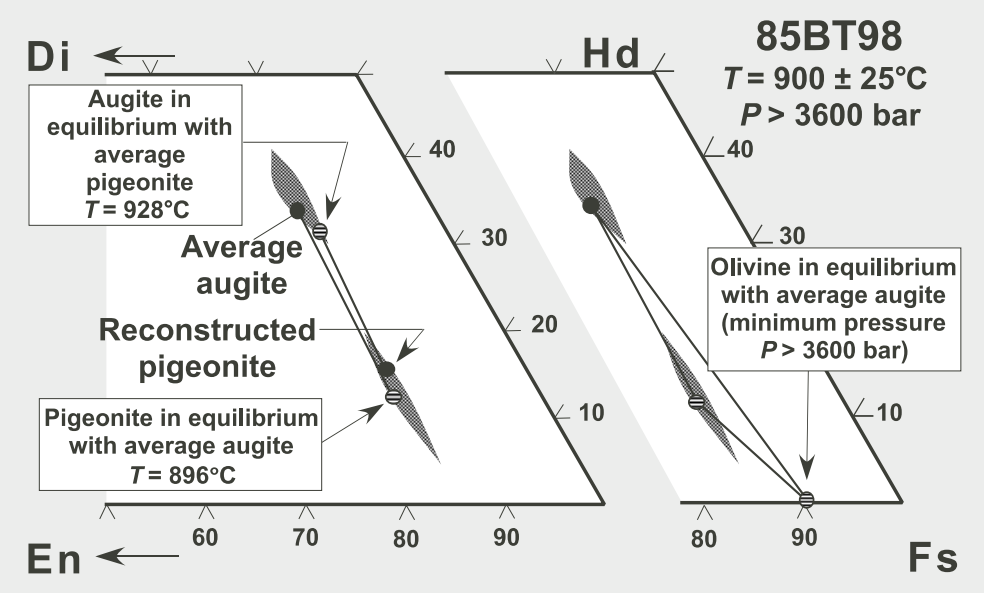

Fig. 15. Pyroxene quadrilateral indicating *P–T* estimates using QUILF-equilibria for sample 85BT98 from the Svarthamaren charnockite (Fig. 3).

Reaction (6) is slightly below QFM at high *T* and above QFM at low *T*. The magnetite-absent reaction defined at the intersection of (5) and (6) is the important biotite-limiting reaction (7).

The common coexistence of biotite + K-feldspar + orthopyroxene requires equilibrium of the reaction

$$2KFe_3AlSi_3O_{10}(OH)_2 + 6SiO_2 = 2KAlSi_3O_8 + 3Fe_2Si2O_6 + 2H_2O. \quad (7)$$

Reaction equilibrium (7) suggests that $aH_2O \sim 0{\cdot}6$ at 900°C and ~0·4 at 800°C and 400 MPa [calculated using data of Berman (1988)]. The calculated aH_2O indicates that the melt crystallized under water-deficient conditions. Orthopyroxene is commonly partially resorbed, suggesting that biotite formed from reaction (7) by fixing the H_2O of the melt during cooling. Also note that the corresponding fayalite-involving reaction is metastable in charnockite because the reaction

$$Fe_2SiO_4 + SiO_2 = Fe_2Si_2O_6 \quad (8)$$

favours the product side, except for extremely Fe-rich compositions. In the extremely Fe-rich fayalite-bearing Qtz-syenites and syenites, the reaction

$$2KFe_3AlSi_3O_{10}(OH)_2 + 3SiO_2 = 2KAlSi_3O_8 + 3Fe_2SiO_4 + 2H_2O \quad (9)$$

is of critical importance. The reaction converts fayalite in the syenitic rocks to biotite with increasing aH_2O. At the inferred temperature of the igneous assemblages of about 900°C, biotite is not stable in fayalite–K-feldspar–Qtz

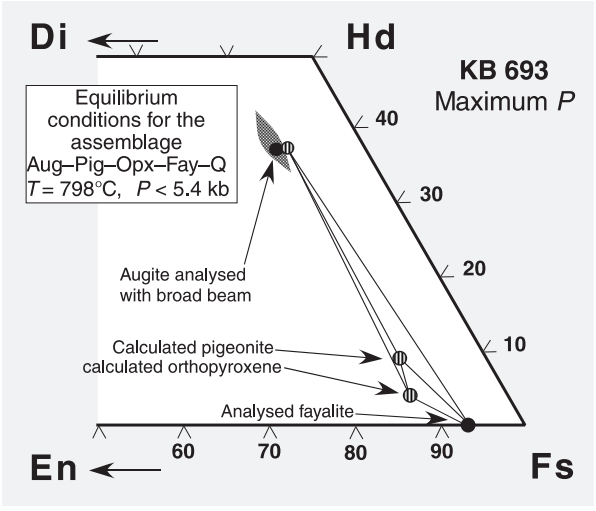

Fig. 16. Pyroxene quadrilateral indicating *P–T* estimates using QUILF-equilibria for sample KB693 from Stålstuten (Fig. 2).

rocks (not even in the presence of melt with $aH_2O = 1$). Consequently, biotite is absent in fayalite-bearing granitoids (Table 1) except for the two alkali-granite dykes. In these, the solidus temperature may have been lower because the high fluorine content possibly fluxed the melt and stabilized biotite. At 800°C, biotite would replace fayalite + K-feldspar in the presence of a fluid (melt, or low-density fluid) if $aH_2O > 0{\cdot}7$ (>0·5 at 700°C). Thus, biotite in the igneous rocks is probably of subsolidus origin, except for the alkali-granitic dyke rocks. During cooling of a magma that produces

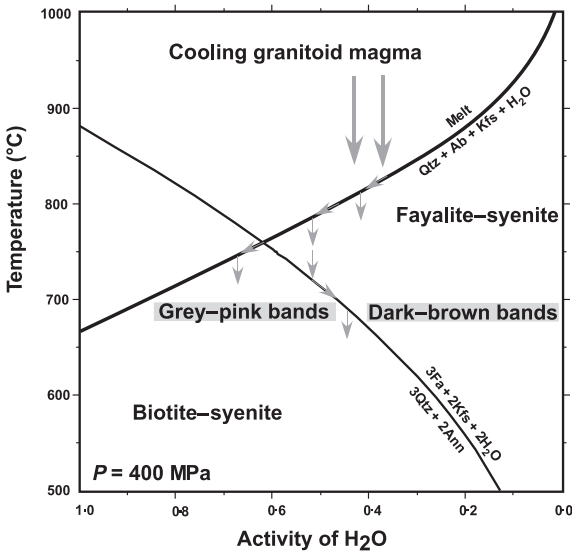

Fig. 17. Temperature versus activity of H_2O diagram showing the equilibrium conditions of the fayalite = biotite reaction (9) in Qtz-syenite [thermodynamic data from Berman (1988)]. Pressure constant at 400 MPa from QUILF thermobarometry and Bucher-Nurminen & Ohta (1993). Granite solidus from Johannes & Holtz (1996). Arrows indicate aH$_2$O evolution trends of igneous rocks during cooling. H_2O buffering by solidus tends to increase aH$_2$O; subsequent biotite formation from fayalite decreases aH$_2$O.

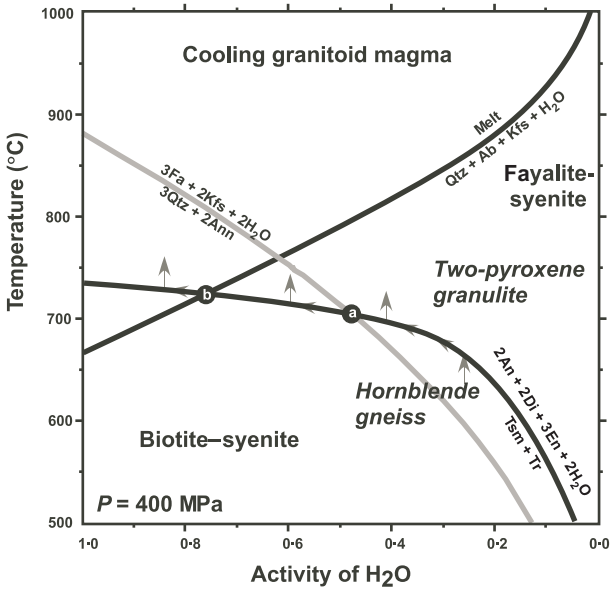

Fig. 18. Temperature versus activity of H_2O diagram showing the equilibrium conditions of the fayalite = biotite reaction (9) in Qtz-syenite and the hornblende breakdown reaction (10) in gneissic xenoliths [thermodynamic data from Berman (1988)]. Pressure constant at 400 MPa from QUILF thermobarometry and Bucher-Nurminen & Ohta (1993). Granite solidus from Johannes & Holtz (1996). Arrows indicate aH$_2$O evolution trends resulting from prograde hornblende decomposition: hornblende dehydration at low aH$_2$O [to the right of point (a)] produces no reaction halos around xenoliths. At intermediate aH$_2$O [between (a) and (b)], fayalite is replaced by biotite in the igneous rocks and results in conspicuous discoloration halos (Fig. 7); at high aH$_2$O [to the left of point (b)] hornblende dehydration would remelt the syenite (not observed).

H_2O-poor assemblages, aH$_2$O increases towards the solidus and aH$_2$O may remain relatively high under subsolidus conditions. From the equilibrium condition of reaction (9) (Fig. 17), it follows that at a given subsolidus temperature (e.g. 800°C, 400 MPa), Qtz-syenite may contain fayalite or biotite, depending on aH$_2$O.

Reactions in the gneissic xenoliths

The textures of the mafic gneisses (Fig. 11) represent evidence for the progress of the prograde amphibole breakdown reaction in these K-feldspar-free rocks:

$$2NaCa_2Fe_4Al_3Si_6O_{22}(OH)_2 + 8SiO_2 = 2CaFeSi_2O_6 + 3Fe_2Si_2O_6 + 2CaAl_2Si_2O_8 + 2NaAlSi_3O_8 + 2H_2O. \quad (10)$$

The decomposition of ferro-pargasitic amphibole produces two pyroxenes and plagioclase and releases H_2O. This archetypal reaction symbolizes the transition from amphibolite- to granulite-facies metamorphism. Progress of this continuously H_2O-releasing reaction is driven by the heat from the high-temperature magmas that enclose the gneissic xenoliths. We suggest that the liberated H_2O migrated from the xenoliths into the enclosing K-feldspar-rich igneous rock, where it had the potential to convert orthopyroxene or fayalite to biotite, according to reactions (7) and (9). The maximum temperature of the xenoliths (~750°C) heated by contact metamorphism is lower than that of the enclosing granite (~800–850°C at the solidus). This requires that prograde amphibole decomposition in the gneiss occurs at lower temperatures than fayalite conversion to biotite in the nearby igneous rocks, which is consistent with the computed reaction equilibria (Fig. 18). The formation of the pink halos around gneiss xenoliths (Fig. 7) is a consequence of biotite decomposing at a higher temperature than amphibole at high aH$_2$O (Fig. 18).

DISCUSSION

The Thor Range plutons are typical anorogenic within-plate granites with all the characteristic features that have been reported for anorogenic granites worldwide (e.g. Ike *et al.*, 1984; Rämö & Haapala, 1995; Frost *et al.*, 1999, 2001, 2002). By analogy with other A-type granites, the Thor Range plutons with their H_2O-poor, high-T, parental magmas may have been generated by extensive partial melting of pre-existing mafic rocks in the lower crust. This may have occurred in relation to crustal

extension (continental break-up) or to a hotspot. In general, other geodynamic settings appear possible (Bonin, 2005; Whalen, 2005), including a late orogenic Pan-African origin of the intrusives as a result of the close time relationship of the plutons to the fading Pan-African orogeny (Henjes-Kunst & Markl, 1998; Engvik & Elvevold, 2004).

The Thor Range charnockites and Fa–Qtz-syenites record pyroxene–fayalite assemblage temperatures close to 900°C and mid-crustal emplacement depths. The solidus temperature of about 800°C is characteristic of H_2O-poor granite magma (Johannes & Holtz, 1996). The high-temperature nature of the granites is preserved because of coarse exsolution in pyroxene permitting reconstruction of the original mineral compositions.

The high halogen content of many rocks and minerals demonstrates that the silicate melt was H_2O-poor and did not form an aqueous fluid phase capable of removing halogens from the rocks at a late stage of magma evolution. The latest granitic dykes are particularly rich in halogens and contain fluorite, which suggests that the halogens were accumulated in the final magma and carried away by silicate melt rather than with an aqueous phase. This also suggests that the magmas did not reach fluid-phase saturation—not even at the very latest stages of cooling or at the solidus.

The striking dark–light bands (Figs 5 and 6) characteristic of the outcrops of the Hochlinfjellet area (Fig. 2) are a consequence of reaction (1) that removed fayalite (and orthopyroxene) from the igneous rocks. Consequently, the rocks cannot later produce iddingsite during low-grade alteration and weathering and stay grey or pink, whereas rocks that were unaffected by fayalite-consuming reactions later developed the characteristic brown iddingsite stain. This also means that none of the outcrops in the Thor Range exposes completely unaltered igneous rocks.

The bulk-rock composition experienced only slight changes during this reaction. An example is the sample pair KB693–KB694 (Table 3). Sample KB693 is a typical brown Fa–Qtz-syenite containing hedenbergite and subordinate hastingsite. Consequently, because halogens are stored in hastingsite, the bulk-rock contains little halogens. Sample KB694 from the same pluton is a pink Qtz-syenite with no fayalite but with abundant hastingsite. Hence, the rock is relatively rich in halogens. The two rocks can be related to the hastingsite-forming reaction (1). It shows that the process creating the discoloured bands within the brown Fa–Qtz-syenite involved hydration and oxidation. It is probably related to a late increase in a_{H_2O} as the cooling magma approaches the solidus (Figs 17 and 18). The increase in a_{H_2O} is accompanied by a passive increase of residual halogens in the melt. The banded structure of high- and low-a_{H_2O} conditions could be a consequence of variations in the local stress field as a result of the emplacement of further plutons in the vicinity. A similar pair of rocks from the alkali-granite intrusions is KB691–KB704. The rocks have essentially the same major element composition (Table 3). However, KB691 is significantly enriched in halogens, suggesting that the rock crystallized from a late melt enriched in halogens.

The plutons are surrounded by contact metamorphic country rocks with assemblages that are typical of 700°C at 500 MPa. The contact metamorphic assemblages indicate low-a_{H_2O} conditions and, where present, a CO_2-rich low-density fluid (Bucher-Nurminen & Ohta, 1993). The charnockite–syenite intrusions disintegrated country rock gneiss and enclosed fragments of various size and shape into the magma. Contact metamorphism heated the fragments up to 750°C. In mafic xenoliths, amphibole decomposed and released H_2O according to reaction (10), corresponding to the microtextures shown in Fig. 11. The H_2O so released migrated into the surrounding igneous rock.

The remarkable pink halos around some of the gneiss xenoliths (Fig. 7) probably formed by a mechanism distinctly different from the one which formed the dark–light bands discussed above (Figs 5 and 6), although the final effect of the different processes that formed the structures is very similar. However, in addition, the pale halos around xenoliths (Fig. 7) and at contacts to basement gneiss also resulted from the interaction of the igneous rocks with H_2O. The hydration of the Fa–Qtz-syenite, as suggested by the structure of the outcrop, may have consumed locally derived H_2O from the gneissic inclusions. The structure displayed in Fig. 7 can be interpreted as follows: the H_2O needed to form pink Bt–Qtz-syenite from Fa–Qtz-syenite by reactions (7) and (9) was provided by the prograde dehydration reaction (10) that was in progress in the gneissic xenoliths. The migration mechanism of H_2O from the xenoliths to the visible hydration front in the enclosing Qtz-syenite (Fig. 7) is uncertain. The fine-grained disequilibrium reaction textures shown in Fig. 11 are typical of fluid-absent conditions. The progressing dehydration reaction probably did not create a fluid phase. Rather, the H_2O produced was lost from the reaction site by grain boundary diffusion. This process is probably fast enough at 700–800°C to reach distances of some metres within the given time-frame.

The occurrence of vein structures (Fig. 7) suggests that a fluid phase was locally present during a very late stage of alteration. The H_2O involved may have been produced by fast dehydration reactions [other than reaction (10), e.g. muscovite decomposition]. The discrete low-density fluid phase probably also contained CO_2 released from the marbles. The fluids travelled along fractures and converted brown Qtz-syenite along centimetre-thick veins into pink granite. The veins advanced by hydraulic fracturing of the solid granite and the vein-forming

process occurred episodically and was very short-lived (Engvik *et al.*, 2003, 2005).

The complete lack of low-grade alteration products, such as chlorite, epidote and muscovite, suggests that the alteration occurred at relatively high temperature or in the presence of a very H_2O-poor fluid phase. Computed assemblage stability diagrams for all bulk-rock compositions in Table 3, using the data of Berman (1988) and the Domino-Theriak software by de Capitani & Brown (1987), predict that the lack of phengite–muscovite in the alteration assemblage at 400 MPa requires a minimum temperature of 600°C in the presence of pure H_2O. At the same pressure, the water-saturated solidus for rocks of relevant composition to this study is close to 640°C (Johannes & Holtz, 1996). A temperature of 620 ± 20°C at 400 MPa and $aH_2O = 1$ for the vein-forming event is thus consistent with the absence of evidence for remelting and the absence of muscovite. In the presence of CO_2 in the low-density fluid, vein alteration may have occurred at lower temperatures without producing muscovite, chlorite or epidote.

CONCLUDING REMARKS

The reaction history recorded by the mineral assemblages of anorogenic granitoids and enclosed gneissic xenoliths bears witness to a subtle interaction of H_2O released and consumed in various volumes of rocks during cooling of the plutons and the heating and cooling cycle of the gneiss xenoliths. Cooling to the solidus of granitic magma takes place in the absence of a low-density fluid. It is accompanied by local hydration of orthopyroxene and fayalite to hastingsite and biotite. Subsolidus fluid-absent dehydration characterizes contact metamorphism of gneiss xenoliths. H_2O produced by dehydration of xenoliths locally hydrated the enclosing igneous rocks and formed characteristic halos around the xenoliths. Finally, fluid-present conditions are indicated by late veins and associated hydration along fractures.

ACKNOWLEDGEMENTS

Fieldwork has been carried out during the Norwegian Antarctic Research Expedition NARE89/90 and we thank all individuals and institutions who made this expedition possible and successful. We are particularly grateful to Yoshihide Ohta for his interest in this work, the companionable fieldwork and for providing thin sections and samples from YO and BT collections, respectively. We also thank Håkon Austrheim for support in the field, exchanging ideas about fluids and granulite genesis and for providing two important samples from his collection. The late M. Frey is thanked for generously providing access to the microprobe in Basel. This research was made possible by German funding: University of Freiburg, Rinne Foundation and von Humboldt Foundation. This support is gratefully acknowledged. The thorough and constructive comments and reviews by Calvin Barnes, Tapani Rämö, Gregor Markl and Marjorie Wilson are gratefully acknowledged. Marjorie Wilson is thanked for her dedicated editorial handling of the manuscript.

REFERENCES

Allen, A. R. (1991). The tectonic and metamorphic evolution of H.U. Sverdrupfjella, western Dronning Maud Land, Antarctica. In: Thomson, M. R. A., Crame, J. A. & Thomson, J. W. (eds) *Geological Evolution of Antarctica*. Cambridge: Cambridge University Press, pp. 53–60.

Andersen, D. J., Lindsley, D. H. & Davidson, P. M. (1993). QUILF: A PASCAL program to assess equilibria among Fe–Mg–Mn–Ti oxides, pyroxenes, olivine, and quartz. *Computers and Geosciences* **19**, 1333–1350.

Berman, R. G. (1988). Internally-consistent thermodynamic data for minerals in the system: Na_2O–K_2O–CaO–MgO–FeO–Fe_2O_3–Al_2O_3–SiO_2–TiO_2–H_2O–CO_2. *Journal of Petrology* **29**, 445–522.

Berman, R. G. (1990). Mixing properties of Ca–Mg–Fe–Mn garnets. *American Mineralogist* **75**, 328–344.

Berman, R. G. (1991). Thermobarometry using multi-equilibrium calculations: a new technique, with petrological applications. *Canadian Mineralogist* **29**, 833–856.

Bonin, B. (2005). A-type granites: definitions, facts and speculations. *Geochimica et Cosmochimica Acta* **69(10S)**, A79.

Bucher, K. & Frost, B. R. (1993). Crystallization history of charnockites, Thor Range, Antarctica: implication to thermobarometry of cordierite gneisses. *GSA meeting Abstract volume* **A-448**.

Bucher, K. & Frost, R. B. (1995). Charnockites and granulites of the Thor range, Queen Maud Land, Antarctica: water recycling in high-grade metamorphism. *Terra Abstracts* **7**, 314.

Bucher-Nurminen, K. & Ohta, Y. (1993). Granulites and garnet–cordierite gneisses from Dronning Maud Land, Antarctica. *Journal of Metamorphic Geology* **11**, 691–703.

Bucher-Nurminen, K., Ohta, Y., Austrheim, H. & Dallmann, W. (1990). Geological observations in Gjelsvikfjella and Mühlig-Hofmannfjella. *Norwegian Polar Research Institute, Meddelelser* **113**, 91–100.

Dallmann, W., Austrheim, H., Bucher-Nurminen, K. & Ohta, Y. (1990). Geology around the Norwegian Antarctic Station 'Troll', Jutulsessen, Dronning Maud Land. *Norsk Polarinstitutt Meddelelser* **111**, 1–39.

de Capitani, C. & Brown, T. H. (1987). The computation of chemical equilibrium in complex systems containing non-ideal solutions. *Geochimica et Cosmochimica Acta* **51**, 2639–2652.

Engvik, A. K. & Elvevold, S. (2004). Pan-African extension and near-isothermal exhumation of a granulite facies terrain, Dronning Maud Land, Antarctica. *Geological Magazine* **141**, 649–660.

Engvik, A. K., Stöckhert, B., Austrheim, H. & Elvevold, S. (2003). Magma-driven hydraulic fracturing and infiltration of CO_2–H_2O fluids into high-grade crystalline rocks, Dronning Maud Land, Antarctica. *Terra Nostra Abstracts* **4**, 82–83.

Engvik, A. K., Bertram, A., Kalthoff, J. F., Stöckhert, B., Austrheim, H. & Elvevold, S. (2005). Magma-driven hydraulic fracturing and infiltration of fluids into the damaged host rock: an example from Dronning Maud Land, Antarctica. *Journal of Structural Geology* **27**, 839–854.

Ferry, J. M. & Spear, F. S. (1978). Experimental calibration of the partitioning of Fe and Mg between garnet and biotite. *Contributions to Mineralogy and Petrology* **66**, 113–117.

Frost, B. R. & Bucher, K. (1993). Charnockites of the Thor Range, Queen Maud Land, Antarctica: the granulite uncertainty principle exemplified. *GSA meeting abstract volume* **A-448**.

Frost, B. R. & Chacko, T. (1989). The granulite uncertainty principle: limitations on thermobarometry in granulites. *Journal of Geology* **97**, 435–450.

Frost, B. R. & Lindsley, D. H. (1992). Equilibria among Fe–Ti oxides, pyroxenes, olivine, and quartz: Part II. Application. *American Mineralogist* **77**, 1004–1020.

Frost, B. R., Barnes, C. G., Collins, W. J., Arculus, R. J., Ellis, D. J. & Frost, C. D. (2001). A geochemical classification for granitic rocks. *Journal of Petrology* **42**, 2033–2048.

Frost, C. D. & Frost, B. R. (1997). Reduced rapakivi-type granites: the tholeiite connection. *Geology* **25**, 647–650.

Frost, C. D., Frost, B. R., Chamberlain, K. R. & Edwards, B. R. (1999). Petrogenesis of the 1·43 Ga Sherman Batholith, SE Wyoming, USA: a reduced rapakivi-type anorogenic granite. *Journal of Petrology* **40**, 1771–1802.

Frost, C. D., Bell, J. M., Frost, B. R. & Chamberlain, K. R. (2001). Crustal growth by magmatic underplating: isotopic evidence from the northern Sherman batholith. *Geology* **29**, 515–518.

Frost, C. D., Frost, B. R., Bell, J. M. & Chamberlain, K. R. (2002). The relationship between A-type granites and residual magmas from anorthosite: evidence from the northern Sherman batholith, Laramie Mountains, Wyoming, USA. *Precambrian Research* **119**, 45–71.

Fuhrman, M. L. & Lindsley, D. H. (1988). Ternary–feldspar modeling and thermometry. *American Mineralogist* **73**, 201–215.

Golynsky, A. & Jacobs, J. (2001). Grenville-age versus Pan-African magnetic anomaly imprints in western Dronning Maud Land, East Antarctica. *Journal of Geology* **109**, 136–142.

Grantham, G. H., Moyes, A. B. & Hunter, D. R. (1991). The age, petrogenesis and emplacement of the Dalmatian granite, H.U. Sverdrupfjella, Dronning Maud Land, Antarctica. *Antarctic Science* **3**, 197–204.

Groenewald, P. B. & Hunter, D. R. (1991). Granulites of northern H.U. Sverdrupfjella, western Dronning Maud Land: metamorphic history from garnet–pyroxene assemblages, coronas and hydration reactions. In: Thomson, M. R. A., Crame, J. A. & Thomson, J. W. (eds) *Geological Evolution of Antarctica*. Cambridge: Cambridge University Press, pp. 61–66.

Haapala, I. & Rämö, O. T. (1992). Tectonic setting and origin of the Proterozoic rapakivi granites of southeastern Fennoscandia. *Transactions of the Royal Society of Edinburgh: Earth Sciences* **83**, 165–171.

Haapala, I. & Rämö, O. T. (1999). Rapakivi granites and related rocks: an introduction. *Precambrian Research* **95**, 1–7.

Henjes-Kunst, F. & Markl, G. (1998). Charnockitic intrusive rocks and related lamprophyres in central Dronning Maud Land, East Antarctic: evidence for long-lasting igneous activities in Late Pan-African times. *Journal of African Earth Sciences* **27**, 110–111.

Holland, T. J. B. & Blundy, J. (1994). Non-ideal interactions in calcic amphiboles and their bearing on amphibole–plagioclase thermometry. *Contributions to Mineralogy and Petrology* **116**, 433–447.

Holland, T. J. B. & Powell, R. (1990). An enlarged and updated internally consistent thermodynamic dataset with uncertainties and correlations: the system K_2O–Na_2O–CaO–MgO–MnO–FeO–Fe_2O_3–Al_2O_3–TiO_2–SiO_2–C–H_2–O_2. *Journal of Metamorphic Geology* **8**, 89–124.

Ike, E. C., Bowden, P. & Martin, R. F. (1984). Fayalite and clinopyroxene in the porphyries of the Tibchi anorogenic ring-complex, Nigeria: postmagmatic initiation of a peralkaline trend. *Canadian Mineralogist* **22**, 401–409.

Jacobs, J., Fanning, C. M., Henjes-Kunst, F., Olesch, M. & Paech, H. J. (1998). Continuation of the Mozambique Belt into East Antarctica: Grenville-age metamorphism and polyphase Pan-African high-grade events in central Dronning Maud Land. *Journal of Geology* **106**, 385–406.

Johannes, W. & Holtz, F. (1996). *Petrogenesis and Experimental Petrology of Granitic Rocks*. Heidelberg: Springer Verlag, 335 pp.

Kohn, M. J. & Spear, F. S. (1989). Empirical calibration of geobarometers for the assemblage garnet–hornblende–plagioclase–quartz. *American Mineralogist* **74**, 77–84.

Kroll, H., Evangelakakis, C. & Voll, C. (1993). Two-feldspar geothermometry, a review and revision for slowly cooled rocks. *Contributions to Mineralogy and Petrology* **114**, 510–518.

Lindsley, D. H. & Frost, B. R. (1992). Equilibria among Fe–Ti oxides, pyroxenes, olivine, and quartz: Part I. Theory. *American Mineralogist* **77**, 987–1003.

Markl, G. & Piazolo, S. (1998). Halogen-bearing minerals in syenites and high-grade marbles of Dronning Maud Land, Antarctica: monitors of fluid compositional changes during late-magmatic fluid–rock interaction processes. *Contributions to Mineralogy and Petrology* **132**, 246–268.

Moyes, A. B. & Groenewald, P. B. (1996). Isotopic constraints on Pan-African metamorphism in Dronning Maud Land, Antarctica. *Chemical Geology* **129**, 247–256.

Moyes, A. B., Barton, J. M. J. & Groenewald, P. B. (1993). Late Proterozoic to Early Palaeozoic tectonism in Dronning Maud Land, Antarctica: supercontinental fragmentation and amalgamation. *Journal of the Geological Society, London* **150**, 833–842.

Ohta, Y. (1993). Nature environment map, Gjelsvikfjella and Western Mühlig-Hofmannfjella, Dronning Maud Land. Antarctica, 1:100 000 sheet 1 and 2. *Norsk Polarinstitutt Temakart* Nr. 24. Oslo: Norsk Polarinstitutt.

Ohta, Y., Tørudbakken, B. O. & Shiraishi, K. (1990). Geology of Gjelsvikfjella and western Mühlig-Hofmannfjella, Dronning Maud Land, east Antarctica. *Polar Research* **8**, 99–126.

Paulsson, O. & Austrheim, H. (2003). A geochronical and geochemical study of rocks from Gjelsvikfjella, Dronning Maud Land, Antarctica: implications for Mesoproterozoic correlations and assembly of Gondwana. *Precambrian Research* **125**, 113–138.

Paulsson, O., Austrheim, H. & Ohta, Y. (1999). Pan-African late orogenic intrusions in Jutulsessen, western Dronning Maud Land, Antarctica. *Journal of Conference Abstracts* **4**, 118.

Pearce, J. A., Harris, N. B. W. & Tindle, A. G. (1984). Trace element discrimination diagrams for the tectonic interpretation of granitic rocks. *Journal of Petrology* **25**, 956–983.

Perchuk, L. L., Aranovich, L. Y., Podlesskii, K. K., Lavrant'eva, I. V., Gerasimov, V. Y., Fed'Kin, V. V., *et al.* (1985). Precambrian granulites of the Aldan shield, eastern Siberia, USSR. *Journal of Metamorphic Geology* **3**, 265–310.

Piazolo, S. & Markl, G. (1999). Humite- and scapolite-bearing assemblages in marbles and calcsilicates of Dronning Maud Land, Antarctica: new data for Gondwana reconstructions. *Journal of Metamorphic Geology* **17**, 91–107.

Rämö, O. T. & Haapala, I. (1995). One hundred years of Rapakivi Granite. *Mineralogy and Petrology* **52**, 129–185.

Ravich, M. G. & Solov'ev, D. S. (1966). Geology and petrology of the mountains of central Queen Maud Land (Eastern Antarctica). *Transactions of the Scientific Research Institute of Arctic Geology, Ministry of Geology, USSR* **141**.

Ravindra, R. & Pandit, M. K. (2000). Geochemistry and geochronology of A-type granite from northern Humboldt Mountain, East Antarctica: vestige of Pan-African Event. *Journal of the Geological Society of India* **56**, 253–262.

Roots, E. F. (1969). Geology of Western Queen Maud Land. *Antarctic Map Folio Series*, Folio 12, Plate VI, American Geographical Society.

Spear, F. S. & Kohn, M. J. (1999). Program Thermobarometry, version 2.1, available online at http//www.geo.rpi.edu/fac-staff/spear/GTP_Prog/GTP.html.

Tingey, R. J. (1991). The regional geology of Archaean and Proterozoic rocks in Antarctica. In: Tingey, R. J. (ed.) *The Geology of Antarctica. Oxford Monographs on Geology and Geophysics*, *17*. Oxford: Clarendon Press. pp. 1–73

Whalen, J. B. (2005). A-type granites: >25 years later. *Geochimica et Cosmochimica Acta*, **69**(10S), A84.